J. Fluid Mech. (2002), *vol.* 456, *pp.* 1–32.
DOI: 10.1017/S0022112001007352 Printed in the United Kingdom

The Boussinesq–Rayleigh approximation for rotational solitary waves on shallow water with uniform vorticity

By VICTOR A. MIROSHNIKOV

Department of Mathematics and Computer Science,
College of Mount Saint Vincent, Riverdale, NY 10471-1093, USA

(Received 24 February 2000 and in revised form 31 July 2001)

The theoretical work reported herein studies the free-surface profile, the flow structure, and the pressure distribution of a finite-amplitude solitary wave on shallow water with uniform vorticity. The kinematic problem for the stream function is formulated employing the vertical coordinate and the free surface as the independent variables of the Poisson equation with variable coefficients that are functions of the Hamiltonian of the rotational solitary wave. The exact solution of the boundary-value kinematic problem for the stream function is derived in the form of a power series complemented by a recurrence relation. The dynamic problems for the Hamiltonian and the free surface are solved globally in the Boussinesq–Rayleigh approximation. To find angles enclosed by the branches of the solution at critical points and points of bifurcation the surface streamline is also treated locally by an exact topological solution. The complete analysis of the four-dimensional Hamiltonian maps presented in §4 specifies critical values of the Froude number and the vorticity for five flow regimes: the emergence of the solitary wave, the flow separation near the bottom, the flow separation near the crest, the critical regime for an instability, and the formation of a limiting configuration. The streamlines of the recirculating flow are obtained as a single-eddy bifurcation that preserves continuity of all derivatives on the boundary streamline. The eddy separated near the crest forms the limiting configuration by blocking the upstream current. The results are compared with weakly nonlinear theory, with numerical simulations and with field observations with satisfactory agreement.

1. Introduction

Surface waves in natural basins usually propagate on shear currents, rather than on still water. For waves of permanent form that occur on running water of finite depth, the assumption of irrotational motion is artificial since the horizontal velocity of the steady stream varies with depth because of the atmosphere–ocean interaction, ocean currents, and the viscous boundary layer. The integral of the steady vorticity transport equation for the inviscid core flow, $\mathrm{D}(\omega,\psi)/\mathrm{D}(X_1,x_3)=0$, states that the vorticity is a function of the stream function only (Lamb 1932). By Taylor's theorem $\omega(\psi)=\omega(\psi_0)+\omega'(\psi_0)(\psi-\psi_0)+\cdots$. Hence, the uniform distribution of vorticity is the next step in the development of a theory of the rotational solitary wave that admits a quite straightforward continuation of the solutions derived for the irrotational solitary wave. As we shall see, the problem considered of the finite-amplitude solitary wave on shallow water with the uniform vorticity is characterized by three independent

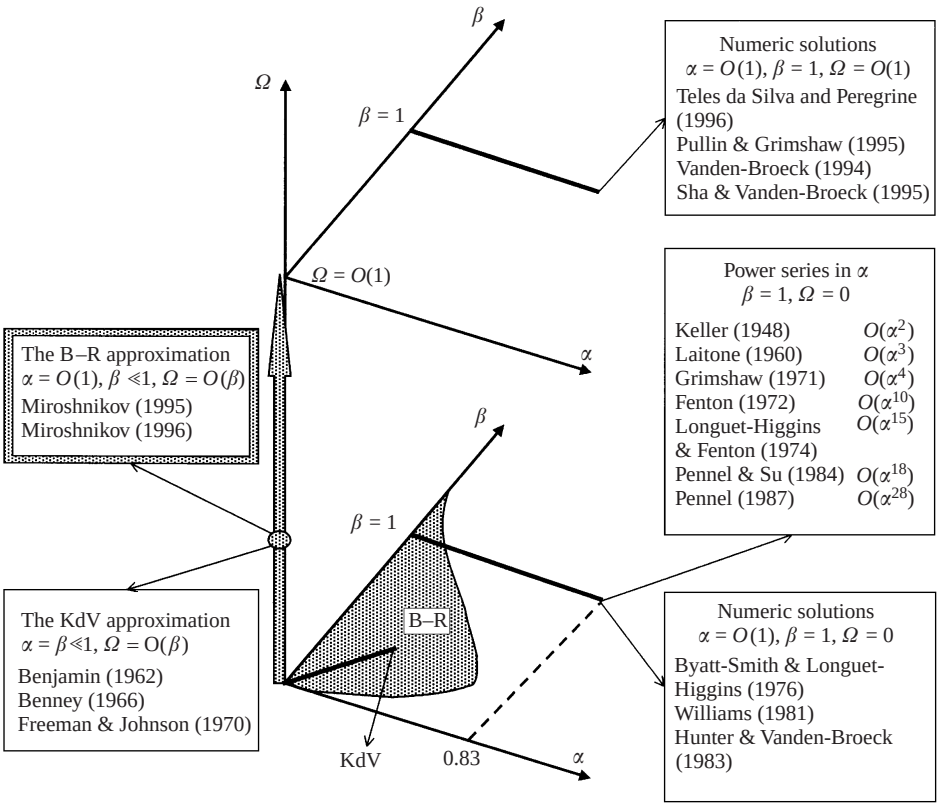

FIGURE 1. Sketch of theories and numerical simulations in the space of parameters of the rotational solitary-wave problem. A rough domain of convergence of the Boussinesq–Rayleigh approximation for the irrotational solitary wave is shaded.

parameters:

$$\alpha = (A - H)/H, \quad \beta = (H/L)^2, \quad \Omega = \omega(\psi_0)H/U_0. \tag{1.1a,b,c}$$

Here, H is a depth of the fluid at infinity, A is an elevation of the crest, α is an amplitude parameter, L is a scale of the horizontal coordinate, β is a shallowness parameter, ω_0 is a constant value of vorticity, U_0 is an absolute velocity on the free surface at infinity in the reference frame moving with the solitary wave, and Ω is a dimensionless vorticity. A sketch of the known theoretical and numerical results in the three-dimensional space of parameters (1.1) is shown in figure 1.

The theory of the irrotational solitary wave has been the object of study of many authors since the pioneering investigations of Boussinesq (1871) and Rayleigh (1876). They developed the shallow water theory using the series expansion for $\alpha = O(1)$ up to $O(\beta^2)$. Korteweg & de Vries (1895) considered the problem in the weakly nonlinear approximation for $\alpha = O(\beta)$ up to $O(\beta^3)$ and initiated many works on interaction of the solitary waves, which are Hamiltonian in this case. See the recent review work by Johnson (1997) for references. Results for the irrotational solitary wave on water of finite depth can be divided in two classes: the series solutions and the numerical solutions. The most developed series solution is the power series in α centred at H for $\beta = 1$ which was calculated up to $O(\alpha^2)$ by Keller (1948), up to $O(\alpha^3)$ by Laitone (1960), up to $O(\alpha^4)$ by Grimshaw (1971), up to $O(\alpha^{10})$ by Fenton (1972),

up to $O(\alpha^{15})$ by Longuet-Higgins & Fenton (1974), up to $O(\alpha^{18})$ by Pennel & Su (1984), and up to $O(\alpha^{28})$ by Pennel (1987). Other types of series were used by Witting (1975), Karabut (1996) and Longuet-Higgins & Fox (1996). The numerical solutions obtained by Byatt-Smith & Longuet-Higgins (1976), Williams (1981) and Hunter & Vanden-Broeck (1983) are mainly based on finite difference approximations of the exact integral equations derived by Milne-Thompson (1968) and Longuet-Higgins (1974).

Note that $\beta = 1$ in all of the above-mentioned works on water of finite depth and the whole two-dimensional parameter space of the irrotational solitary wave is not fully described. So, the Boussinesq–Rayleigh approximation provides the largest domain of convergence among the analytic solutions for the irrotational solitary wave. A similar approximation was recently developed for the internal steady and unsteady waves (see Derzho & Grimshaw 1997 and references therein). They showed that the small value of the Boussinesq parameter allows the construction of the finite-amplitude rotational solitary waves.

Theoretical work on waves propagating on non-uniform currents is reviewed in Peregrine (1976) and Craik (1985). The rotational solitary wave on the shallow stream with an arbitrary distribution of vorticity was studied by Benjamin (1962) in the Korteweg–de Vries (KdV) approximation for $\alpha = \beta$ up to $O(\beta^2)$. Benney (1966) and Freeman & Johnson (1970) presented an alternative derivation of Benjamin's results and showed that the rotational solitary wave is the Hamiltonian system in the KdV approximation. The highly nonlinear solitary waves on water of finite depth with constant vorticity were considered numerically by Teles da Silva & Peregrine (1988), Pullin & Grimshaw (1988), Vanden-Broeck (1994), and Sha & Vanden-Broeck (1995) for $\beta = 1$ by the surface integral equation method. Teles da Silva & Peregrine (1988) showed that the rotational solitary waves exist both for positive and negative vorticity, calculated the integral properties of the solitary waves, and demonstrated that the far upstream flow separates from the bottom beneath the crest for negative vorticity if α is large enough. For highly nonlinear periodic waves with negative vorticity, the pressure beneath the wave crest drops below the atmospheric value and a pressure instability occurs. Vanden-Broeck (1994) found the critical value of vorticity Ω_c such that α is unbounded for $\Omega < \Omega_c$, calculated the solitary wave in the absence of gravity, and constructed the new family of solutions. Pullin & Grimshaw (1988), Sha & Vanden-Broeck (1995) and Vanden-Broeck (1995, 1996) considered numerically new families of periodic and solitary waves in one-layer and two-layer fluids. Miroshnikov (1996) solved the problem analytically for the finite-amplitude rotational solitary wave on the shallow stream with weak linear vorticity in the Boussinesq–Rayleigh approximation for $\alpha = O(1)$ and $\Omega = O(\beta)$ up to $O(\beta^2)$ and showed that there is the critical value of α such the flow separates near the crest in the supercritical regime. It was also shown that the flow separation can be controlled by the electromagnetic force for the solitary wave propagating on the shallow stream of electrolyte (Miroshnikov 1995).

The main difference between the rotational solitary wave and the irrotational one is formation of eddies at high α. This feature crucially alters the kinematic nature of the wave motion. The irrotational solitary wave is a quasi-kinematic object that does not perform a large-scale transfer of mass, except the drift $\delta = O(\alpha^{1/2})$ (Fenton 1972), but the rotational solitary wave does transfer the mass of the separated eddy in the supercritical regime of flow separation (Miroshnikov 1999). This interesting property of the rotational solitary wave has also attracted the attention of investigators of an internal solitary wave in continuously stratified fluids where vorticity is generated

by the internal wave (see Brown & Christie 1998; Derzho & Grimshaw 1997 and references therein).

The main goals of the present work are the following: (*a*) to develop the exact series solution of the kinematic boundary-value problem for the finite-amplitude solitary wave on shallow water with constant vorticity, (*b*) to show that the rotational solitary wave is a Hamiltonian system to any order in β, (*c*) to find the Hamiltonian in the Boussinesq–Rayleigh approximation for $\alpha = O(1)$ and $\Omega = O(1)$ up to $O(\beta^2)$, (*d*) to extend the Boussinesq–Rayleigh solution for the solitary wave on shallow water with constant vorticity, (*e*) to study critical parameters and topological properties of the single-eddy bifurcation, (*f*) to explore the pressure instability of the resulting coherent wave–vortex structures, and (*g*) to compare the obtained theoretical results with the weakly nonlinear theories, with the numerical simulations, and with the field observations.

The remainder of this paper is structured as follows. The kinematic problem for the nonlinear rotational solitary with recirculating flow is set up in § 2 using the vertical coordinate and the free surface as the independent variables of the Poisson equation, with the coefficients depending on the Hamiltonian of the rotational solitary wave and its derivative. The dynamic problem is also formulated in the same variables. The exact solution of the kinematic problem is derived in the form of the power series in β complemented by the recurrence relation in § 3. The boundary-value problem for the stream function is solved exactly and an exact differential equation of infinite order for the dynamic boundary condition is derived in the next section. The Hamiltonian of the rotational solitary wave is obtained and the four-dimensional Hamiltonian maps are studied in detail in § 4 to find critical parameters for the four flow regimes: the emergence of the rotational solitary wave, the separation of the single vortex eddy near the bottom, the separation of the single vortex near the crest, and the formation of the limiting configuration. The previous theoretical and numerical results are confirmed and extended. The admissible profiles of the free surface and the blocking of the upstream current by the limiting configuration are considered here, as well. In § 5 the detailed study of properties of the eddy separated by the single-eddy bifurcation is tackled and we find that streamlines bifurcate preserving continuity of all derivatives. The distribution of pressure is obtained in § 6 and we find the critical flow regime for the pressure instability. The results are compared with field observations with satisfactory agreement. A summary and concluding remarks are given in § 7. In the Appendix, the previous results on the limiting angle of 120° for the rotational solitary wave by Milne-Thompson (1968) and Delachenal (1973) are extended by the exact topological solution in the immediate neighbourhood of the point of bifurcation. The solution shows that the angle enclosed by two bifurcating branches is 60°.

2. Formulation

A two-dimensional solitary wave is supposed to occur upon a non-uniform stream of an inviscid fluid with constant density. The stream is assumed to be rotational and characterized by a uniform vorticity ω_0. Following the Boussinesq–Rayleigh formulation developed by Lamb (1932, §§ 252, 253), we take a frame of reference with the x_1-axis along the horizontal bottom and with gravity acting in the $-x_3$-direction. The horizontal and vertical velocity components, the stream function, and the pressure are v_1, v_3, ψ_2, and p, respectively. Let c denote the absolute speed of the solitary wave that, without loss of generality, propagates in the x_1-direction. On the assumption that the solitary wave propagates without change of form, the problem can be treated

as one of steady motion by taking the reference frame ($X_1 = x_1 - ct, x_3$) moving horizontally with the wave. Then the variables of the moving frame, designated by capital letters, are given by

$$(V_1, V_3, \Psi_2, P)(X_1, x_3) = (v_1 - c, v_3, \psi_2 + cx_3, p)(x_1, x_3, t). \tag{2.1}$$

We adopt a multiscale scheme of dimensionless variables in which H is taken as the scale of $x_3 = Hz$, L is taken as the scale of $x_1 = Lx$ and $X_1 = LX$, U_0 is taken as the scale of $v_1 = U_0 u$, $V_1 = U_0 U$, $v_3 = U_0 w$, and $c = U_0 C$, $U_0 H$ is taken as the scale of $\psi_2 = U_0 H\psi$ and $\Psi_2 = U_0 H\Psi$, U_0/H is taken as the scale of $\omega_0 = U_0\Omega/H$. By definition

$$U = -\frac{\partial \Psi}{\partial z}, \quad w = \beta^{1/2}\frac{\partial \Psi}{\partial X}, \tag{2.2a,b}$$

$$\Omega = \frac{\partial U}{\partial z} - \beta^{1/2}\frac{\partial w}{\partial X} = -\left(\frac{\partial^2 \Psi}{\partial z^2} + \beta\frac{\partial^2 \Psi}{\partial X^2}\right) = -\nabla^2 \Psi. \tag{2.3}$$

To find the primary plane parallel flow at the upstream infinity ($X \to \infty$), we assume that its stream function depends only on z and solve (2.3) with the following boundary conditions: $\Psi_p(0) = 0$ and $\Psi_p'(1) = 1$, where the first condition sets the reference value for Ψ_p and the second condition specifies the direction of propagation. The far upstream condition is then

$$X \to \infty, \quad \Psi \to \Psi_p = (1 + \Omega)z - \tfrac{1}{2}\Omega z^2. \tag{2.4}$$

This linear primary current $U_p = -\Psi_p' = -1 + \Omega(z - 1)$ was used by Vanden-Broeck (1994) to consider the solitary wave in water of finite depth with constant vorticity. Note that the primary stream becomes uniform when $\Omega = 0$.

The velocity of the primary flow in the moving frame is given in figure 2(a) for both negative and positive vorticity. The most important property of the primary flow is that the unidirectional flow becomes bidirectional if $\Omega < -1$. We restrict the further analysis to $\Omega \geqslant -1$ to avoid instability. As we shall see, this restriction also follows from our investigation the Hamiltonian of the rotational solitary wave. Benjamin (1962) arrived at the same conclusion in his study of the weakly nonlinear rotational solitary wave.

Although in a real fluid the velocity must vanish on the channel bottom, and the rate of shearing must vanish on the free surface, these conditions do not have to be applied to the inviscid model considering the core flow at high Reynolds numbers outside the viscous boundary layer. Following the formulation of the previous papers on the linear-vorticity solitary waves (Miroshnikov 1995, 1996), we use the non-slip condition on the channel bottom to construct a more realistic approximation to the primary flow and to resolve ambiguity for C. Hence $u_p = \Omega z$ and $C = 1 + \Omega$, i.e. the irrotational solitary wave propagates on still water under the given condition. So the rotational solitary wave propagates against the current for $\Omega < 0$ and it propagates with the current if $\Omega > 0$.

In the Boussinesq–Rayleigh method, the kinematic conditions are used in the integral form. Namely, $\Psi(X, z)$ is constant on the channel bottom and on the free surface because both boundaries coincide with the streamlines. The unknown constants are determined by the primary flow as

$$\Psi(X, 0) = 0, \quad \Psi(X, s(X)) = 1 + \frac{1}{2}\Omega, \tag{2.5}$$

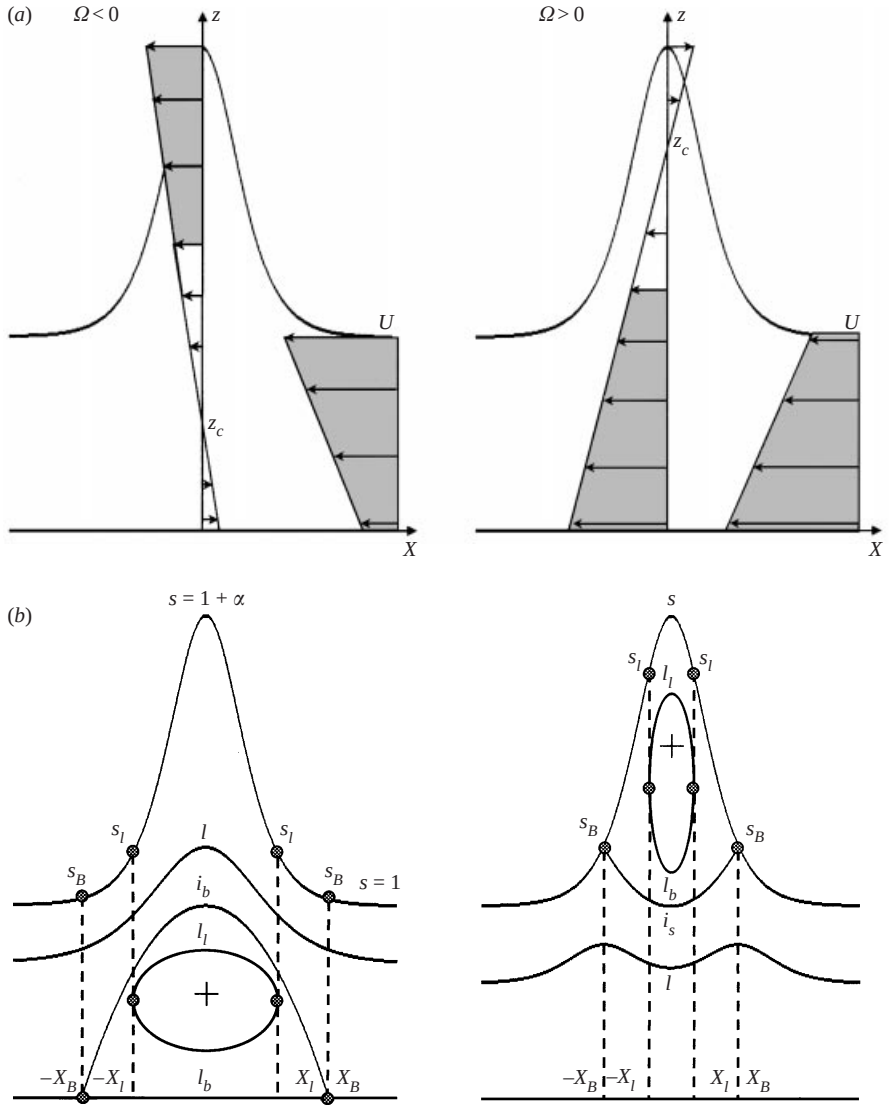

FIGURE 2. (*a*) Illustration of the flow separation in the solitary wave on a stream with constant vorticity in a frame of reference moving with the wave. (*b*) Definition sketches of the streamline pattern associated with the single-vortex bifurcation that appears in (2.7) and (2.8).

where $s(X)$ denotes the elevation of the wave above the channel bottom. To specify that the wave must be a solitary wave, we complement (2.5) by

$$X \to \pm\infty, \quad s(X) \to 1. \tag{2.6}$$

Note that that the requirement of the symmetry of the solitary wave with respect to the z-axis is not necessary because the Hamiltonian of the rotational solitary wave admits only symmetrical phase trajectories satisfying (2.6) (see § 4).

In the numerical simulation by Teles da Silva & Peregrine (1988) and in the weakly vortical theories by Miroshnikov (1995, 1996), it was shown that the separation of the steady flow inside the rotational solitary wave is possible if α is large enough. This effect was qualitatively discussed in detail by Benjamin (1966, § 2) but he neglected the

flow separation as non-treatable in the frames of the weakly nonlinear theory. The separated solitary-wave flow given in figure 2(*a*, *b*) is similar to a steady duct flow in a channel with the cavity corresponding to the crest of the rotational solitary wave. The separation of a viscous flow in channels with curved walls is well documented. The Görtler eddies are generated on the curved wall because of the viscous braking if α and the Reynolds number, which corresponds to the Froude number in the case of solitary waves, are high enough. The inviscid braking of the solitary-wave flow is caused by two factors: (i) the kinematic braking, in agreement with the mass conservation law; and (ii) the dynamic braking, in line with the energy conservation law. First, compare two plane parallel velocity profiles of the solitary-wave stream at $X = 0$ and $X = \infty$, as given in figure 2(*a*), where the elevation of the solitary-wave flow is $1 + \alpha$ and 1, respectively. As the total flux is constant, increasing s will decrease an average value of the horizontal velocity, which can locally become negative. The location of zones with the recirculating flow depends on the sign of Ω. For $\Omega < 0$, the recirculating zone is located near the channel bottom and it is located near the crest of the rotational solitary wave if $\Omega > 0$. Second, compare the velocities on the free surface at $X = 0$ and $X = \infty$. By the Bernoulli law, $U_0^2 U^2(0, 1+\alpha)/2 + gH(1+\alpha) = U_0^2/2 + gH$ (where g is the gravitational acceleration). As the total energy of the fluid particle is constant, an increase in α will diminish the velocity on the crest.

To include the recirculating flow in the formulation of the kinematic problem, we consider a single stream function of the coherent wave–vortex structure which describes the wavy flow by single-valued streamlines and the recirculating flow by two-valued streamlines shown in figure 2(*b*). The single-valued streamline $z = l(X)$ is a solution of $\Psi(X, z) = \Psi_0$, where $0 < \Psi_0 < 1 + \Omega/2$ in agreement with (2.5). When Ψ_0 reaches the boundary value, the streamline bifurcates on the interval $|X| < X_B$ into two branches:

$$\left.\begin{array}{lll} \Omega < 0, \quad \Psi_0 = 0, & z = \left\{ \begin{array}{ll} i_b(X), 0 & \text{when } |X| \leqslant X_B, \\ 0 & \text{when } |X| \geqslant X_B, \end{array} \right. \\ \Omega > 0, \quad \Psi_0 = 1 + \Omega/2, & z = \left\{ \begin{array}{ll} s(X), i_s(X) & \text{when } |X| \leqslant X_B, \\ s(X) & \text{when } |X| \geqslant X_B, \end{array} \right. \end{array}\right\} \tag{2.7}$$

where $i_b(\pm X_B) = 0$, $i_s(\pm X_B) = s(\pm X_B)$, X_B being the half-width of the recirculating zone. The boundaries of the recirculating zone near the channel bottom are given by $z = i_b(X)$ and $z = 0$, where $|X| \leqslant X_B$ and $\Omega < 0$, and the boundaries of the recirculating zone near the crest are given by $z = s(X)$ and $z = i_s(X)$, where $|X| \leqslant X_B$ and $\Omega > 0$. The streamlines of the recirculating flow are two solutions of $\Psi(X, z) = \Psi_0$:

$$\left.\begin{array}{l} \Omega < 0, \quad \Psi_0 < 0, \\ \Omega > 0, \quad \Psi_0 > 1 + \Omega/2, \end{array}\right\} \quad z = \{l_t(X), l_b(X)\} \quad \text{when } |X| \leqslant X_l, \tag{2.8}$$

where $l_t(\pm X_l) = l_b(\pm X_l)$, X_l is the half-width of the zone bounded by $z = l_s(X)$ and $z = l_b(X)$. Maximal and minimal values of Ψ_0 give the flux of the separated eddies for $\Omega > 0$ and $\Omega < 0$, respectively. Similar to the problem of an irrotational solitary wave, the variables $s(X)$, $i_b(X)$, $i_s(X)$, $l_b(X)$, $l_t(X)$, Ψ_0, X_B, and X_l are unknowns of the dynamic problem. Using the novel exact topological solution in the Appendix, it is proved that the angle between $s(X)$ and $i_s(X)$ at the point of bifurcation $X = \pm X_B$ is equal to 60° for the recirculating flow and it is demonstrated that the angle is equal to 120° for the wavy flow, in agreement with Milne-Thompson (1968) and Delachenal (1973). This bifurcation may be called a single-eddy bifurcation. The most important

property of the single-eddy bifurcation is that all derivatives of the single-valued stream function are continuous on the separating streamlines $i_b(X)$ and $i_s(X)$.

We assume that the rotational solitary wave is a one-dimensional, nonlinear Hamiltonian system with a Hamiltonian $H = s'/2 + \Pi(s)$, where $\Pi(s)$ is a potential energy, s' is a momentum and a phase mass is equal to one. This assumption is justified *a posteriori* in §4. As the Hamiltonian does not depend on time explicitly, the total energy is the integral of motion

$$\frac{1}{2}\left(\frac{\mathrm{d}s}{\mathrm{d}X}\right)^2 + \Pi(s) = 0, \tag{2.9}$$

where a constant of integration is included in $\Pi(s)$. Equation (2.9) can be thought of as the energy conservation law for a particle of unit mass moving in a potential well. From this point of view the coordinate X is an analogue of a phase time and the elevation s is an analogue of a phase coordinate, $s'/2$ represents the particle kinetic energy $K(s) = -\Pi(s)$, $\Pi(s)$ represents the potential well, and the total energy of the particle may be always set to zero by selecting the appropriate value of $\Pi(s)$. It is well-known that (2.9) always may be integrated implicitly as $X - X_0 = \int(-2\Pi)^{-1/2}\mathrm{d}s$. This integration yields that the problem is naturally parameterized by $X = X(s)$, where $1 \leqslant s \leqslant 1+\alpha$. Although the Boussinesq–Rayleigh solution is based on the explicit form of the free surface $z = s(X)$, the numeric simulations of the rotational solitary wave by Simmen & Saffman (1985), Teles da Silva & Peregrine (1988), Pullin & Grimshaw (1988), Vanden-Broeck (1994), Sha & Vanden-Broeck (1995) used the parameterized free surface to allow for multi-valued solutions. The parameterization proposed here allows us to readily combine an explicit form of the stream function obtained by the Boussinesq–Rayleigh method with the implicit double-valued streamlines required for the single-eddy bifurcation.

Using (s, z) as new independent variables, we rewrite the kinematic problem (2.3), (2.5), (2.7), (2.8) for $\Psi(s, z)$ as follows:

$$\frac{\partial^2\Psi}{\partial z^2} + \beta\left[2K(s)\frac{\partial^2\Psi}{\partial s^2} + \frac{\mathrm{d}K}{\mathrm{d}s}\frac{\partial\Psi}{\partial s}\right] = -\Omega, \tag{2.10}$$

$$\Psi(s,0) = 0, \quad \Psi(s,s) = 1 + \tfrac{1}{2}\Omega, \tag{2.11}$$

$$\left.\begin{array}{ll} \Omega < 0, \quad \Psi_0 = 0, & z = \left\{\begin{array}{ll} i_b(s), 0 & \text{when } s_B \leqslant s \leqslant 1+\alpha, \\ 0 & \text{when } 1 \leqslant s \leqslant s_B, \end{array}\right. \\ \Omega > 0, \quad \Psi_0 = 1 + \Omega/2, & z = \left\{\begin{array}{ll} s, i_s(s) & \text{when } s_B \leqslant s \leqslant 1+\alpha, \\ s & \text{when } 1 \leqslant s \leqslant s_B, \end{array}\right. \end{array}\right\} \tag{2.12}$$

$$\left.\begin{array}{l} \Omega < 0, \quad \Psi_0 < 0, \\ \Omega > 0, \quad \Psi_0 > 1 + \Omega/2, \end{array}\right\} \quad z = \{l_t(s), l_b(s)\} \quad \text{when } s_l \leqslant s \leqslant 1+\alpha, \tag{2.13}$$

where $s_B = s(X_B)$ and $s_l = s(X_l)$.

In the reference frame moving with the wave, the pressure is determined by the Bernoulli integral, which for an inviscid steady flow with an arbitrary distribution of vorticity is (Milne-Thompson 1968 §4.5; Miroshnikovs 1996; Miroshnikov 1998)

$$\frac{1}{2}\left[\left(\frac{\partial\Psi_2}{\partial X_1}\right)^2 + \left(\frac{\partial\Psi_2}{\partial x_3}\right)^2\right] + \frac{p}{\rho} + gx_3 + \int_{\Psi_S}^{\Psi_2}\omega_2(\Psi)\,\mathrm{d}\,\Psi = E(\Psi_S), \tag{2.14}$$

where E is the Bernoulli energy, ρ is the fluid density and Ψ_S is a reference value

of the stream function on the free surface. Let p_0 denote the atmospheric pressure, $\omega_2(\Psi)$ be the uniform vorticity ω_0, then integrating (2.14) we have

$$\frac{1}{2}\left[\left(\frac{\partial \Psi_2}{\partial X_1}\right)^2+\left(\frac{\partial \Psi_2}{\partial x_3}\right)^2\right]+\frac{p}{\rho}+gx_3+\omega_0\left(\Psi_2-U_0H-\frac{\omega_0 H}{2}\right)=\frac{U_0^2}{2}+\frac{p_0}{\rho}+gH. \tag{2.15}$$

Taking ρgH as the scale of $p-p_0=\rho gHP$, using the Froude number $F=U_0/(gH)^{1/2}$ and parameterizing the free surface, we obtain

$$P(s,z)=1-z+\frac{F^2}{2}\left[1-2\beta K(s)\left(\frac{\partial \Psi}{\partial s}\right)^2-\left(\frac{\partial \Psi}{\partial z}\right)^2\right]+F^2\Omega\left(1+\frac{\Omega}{2}-\Psi\right). \tag{2.16}$$

This is the pressure equation calculated in terms of the stream function and the Hamiltonian. If solutions of the kinematic and free-surface problems are obtained, then (2.16) solves the pressure problem. On the free surface, the pressure equation combined with the differential form of the kinematic boundary condition (2.11) and the condition $P(s,s)=0$ yields

$$[1+2\beta K(s)]\left(\frac{\partial \Psi}{\partial z}\right)^2_{z=s}+\frac{2(s-1)}{F^2}=1. \tag{2.17}$$

The present formulation of the mathematical problem of the rotational solitary wave differs from the known formulations in two respects: (i) the explicit consideration of the flow separation by the single-eddy bifurcation is novel, and (ii) the parameterization of the free surface displaying the Hamiltonian properties of the rotational solitary wave was not used in the previous theories.

3. Stream function

Following the Boussinesq–Rayleigh method, we look for a solution of (2.10) with $\Omega=0$ satisfying the kinematic condition on the bottom in the form of a power series in β:

$$\begin{aligned}\Psi &= U_1(s)z+\beta U_2(s)\frac{z^2}{2!}+\beta U_3(s)\frac{z^3}{3!}+\beta^2 U_4(s)\frac{z^4}{4!}+\beta^2 U_5(s)\frac{z^5}{5!}+\cdots\\ &= U_1(s)z+\sum_{n=1}^{\infty}\beta^n\left[U_{2n}(s)\frac{z^{2n}}{(2n)!}+U_{2n+1}(s)\frac{z^{2n+1}}{(2n+1)!}\right],\end{aligned} \tag{3.1}$$

and assume that the series converges in some interval $0<\beta<\beta_1$. Note that the shallowness parameter is not necessarily small. For $\beta=1$, (3.1) becomes the solution of a finite-depth problem. If β is small enough, one may neglect terms of higher order in β and find an asymptotic solution of a shallow-water problem. Differentiating (3.1) with respect to z and s and substituting in (2.10) gives

$$\sum_{n=1}^{\infty}\beta^{n+1}\frac{z^{2n+1}}{(2n+1)!}\left[U_{2n+3}+\mathrm{D}_s^{(2)}U_{2n+1}\right]+\beta U_2+\sum_{n=1}^{\infty}\beta^{n+1}\frac{z^{2n}}{(2n)!}\left[U_{2n+2}+\mathrm{D}_s^{(2)}U_{2n}\right]=0,$$

where $\mathrm{D}_s^{(2)}$ is a nonlinear differential operator defined by

$$\mathrm{D}_s^{(2n)}=2K(s)\frac{\mathrm{d}^{2n}}{\mathrm{d}s^{2n}}+\frac{\mathrm{d}K}{\mathrm{d}s}\frac{\mathrm{d}}{\mathrm{d}s},\quad n=0,1,2,3,\ldots. \tag{3.2}$$

For (2.10) to be satisfied for all β, Ω, s and z, the coefficients of each power of z must be zero. Hence, the recurrence relations are

$$\left.\begin{aligned} U_2 = 0, \quad & U_{2n+2} + \mathrm{D}_s^{(2)} U_{2n} = 0, \qquad n = 1, 2, 3, \ldots, \\ & U_{2n+3} + \mathrm{D}_s^{(2)} U_{2n+1} = 0, \quad n = 0, 1, 2, 3, \ldots . \end{aligned}\right\} \tag{3.3}$$

The even-numbered coefficients vanish identically. Solving the recurrence relation for the odd-numbered coefficients, substituting these coefficients into (3.1) and adding the partial solution of (2.10), we have

$$\begin{aligned} \Psi &= -\Omega(s)\frac{z^2}{2!} + U_1(s)z - \beta\frac{z^3}{3!}\mathrm{D}_s^{(2)}U_1 + \beta^2\frac{z^5}{5!}\mathrm{D}_s^{(4)}U_1 - \beta^3\frac{z^7}{7!}\mathrm{D}_s^{(6)}U_1 + \cdots \\ &= -\Omega(s)\frac{z^2}{2!} + \sum_{n=1}^{\infty}(-1)^n\beta^n\frac{z^{2n+1}}{(2n+1)!}\mathrm{D}_s^{(2n)}U_1. \end{aligned} \tag{3.4}$$

If we put $\Omega = 0$, retain terms of $O(\beta)$ and replace differentiation with respect to s with differentiation with respect to X, (3.4) reduces to the Boussinesq–Rayleigh solution (Lamb 1932, § 252). As one of the kinematic conditions is satisfied, the stream function is determined up to a single arbitrary function $U_1(s)$, which represents the absolute value of the velocity on the bottom.

To find the Boussinesq–Rayleigh solution of the boundary-value problem (2.10)–(2.11) up to $O(\beta^2)$ the method of successive approximations was used. The same result may be derived by the asymptotic expansion in β (Miroshnikov 1996). In this paper, we look for the exact solution of the kinematic boundary-value problem in the form of a power series in β

$$U_1(s) = p_0(s) + \beta p_1(s) + \beta^2 p_2(s) + \beta^3 p_3(s) + \cdots = \sum_{n=0}^{\infty}\beta^n p_n(s), \tag{3.5}$$

and assume that the series converges in some interval $0 < \beta < \beta_2$. Here p_0 is a single independent function corresponding to U_1. It will be shown that p_0 is the generating function of the series for U_1 and that it is connected with p_n by a recurrence relation. Substituting (3.5) for U_1 in (3.4) and using the free-surface condition of (2.11), we obtain

$$-\Omega\frac{s^2}{2!} + sp_0 + \sum_{n=1}^{\infty}\beta^n\sum_{k=0}^{n}(-1)^k\frac{s^{2k+1}}{(2k+1)!}\mathrm{D}_s^{(2k)}p_{n-k} = 1 + \tfrac{1}{2}\Omega. \tag{3.6}$$

In the irrotational case, this equation written in Cartesian coordinates coincides with the nonlinear boundary-value operator equation for the irrotational solitary wave obtained by Fenton (1972, equation (8a)). For this kinematic boundary condition to be satisfied for all β, Ω and s, the coefficients of each power of β must vanish. This condition yields

$$p_0 = (1 + \Omega/2)/s + \Omega s/2 \tag{3.7}$$

and the following recurrent relations for $n \geqslant 1$:

$$p_1 = \frac{s^2\mathrm{D}_s^{(2)}p_0}{3!}, \quad p_2 = \frac{s^2\mathrm{D}_s^{(2)}p_1}{3!} - \frac{s^4\mathrm{D}_s^{(4)}p_0}{5!}, \quad p_3 = \frac{s^2\mathrm{D}_s^{(2)}p_2}{3!} - \frac{s^4\mathrm{D}_s^{(4)}p_1}{5!} + \frac{s^6\mathrm{D}_s^{(6)}p_0}{7!}, \ldots,$$

$$p_n = \sum_{k=1}^{n}(-1)^{k+1}\frac{s^{2k}}{(2k+1)!}\mathrm{D}_s^{(2k)}p_{n-k}. \tag{3.8}$$

Substituting (3.8) for p_n into (3.5) and the result into (3.4), we find the stream function

of the rotational solitary wave on the stream with uniform vorticity,

$$\begin{aligned}\Psi &= z\left\{\left(1+\frac{\Omega}{2}\right)\frac{1}{s}+\frac{\Omega}{2}(s-z)+\beta\frac{(s^2-z^2)}{3!}\mathrm{D}_s^{(2)}p_0\right.\\&\quad+\beta^2\left[\frac{(s^2-z^2)}{3!}\mathrm{D}_s^{(2)}p_1-\frac{(s^4-z^4)}{5!}\mathrm{D}_s^{(4)}p_0\right]\\&\quad\left.+\beta^3\left[\frac{(s^2-z^2)}{3!}\mathrm{D}_s^{(2)}p_2-\frac{(s^4-z^4)}{5!}\mathrm{D}_s^{(4)}p_1+\frac{(s^6-z^6)}{7!}\mathrm{D}_s^{(6)}p_0\right]+\cdots\right\}\\&= z\left[\left(1+\frac{\Omega}{2}\right)\frac{1}{s}+\frac{\Omega}{2}(s-z)+\sum_{n=1}^{\infty}\beta^n\sum_{k=1}^{n}(-1)^k\frac{s^{2k}-z^{2k}}{(2k+1)!}\mathrm{D}_s^{(2k)}p_{n-k}\right],\end{aligned}\tag{3.9}$$

where p_0 and p_n are given by (3.7) and (3.8), respectively. The kinematic boundary conditions on the bottom ($z=0$) and on the free surface ($z=s$) are obviously satisfied. As $s\to 1$, the stream function of the rotational solitary wave approaches the stream function of the primary flow (2.4). If we consider a primary flow with weak vorticity $\Omega=-\beta\delta_0$, retain terms of $O(\beta)$ and replace $\mathrm{D}_s^{(2k)}$ with differentiation with respect to X, then (3.9) coincides with the previous result by Miroshnikov (1996) with $\delta_1=0$.

4. Hamiltonian

According to (2.2*a*), (3.7)–(3.9), the dynamic boundary condition (2.17) nonlinearly depends on the horizontal velocity on the free surface

$$U_s(s)=q_0(s)+\beta q_1(s)+\beta^2 q_2(s)+\beta^3 q_3(s)+\cdots=\sum_{n=0}^{\infty}\beta^n q_n(s),\tag{4.1}$$

where $q_0(s)$ is the generating function,

$$q_0=-(1+\Omega/2)/s+\Omega s/2,\tag{4.2}$$

and the $q_n(s)$ are determined for $n\geqslant 1$ by the following recurrence relations:

$$\begin{aligned}q_1&=\frac{2s^2\mathrm{D}_s^{(2)}p_0}{3!},\\q_2&=\frac{2s^2\mathrm{D}_s^{(2)}p_1}{3!}-\frac{4s^4\mathrm{D}_s^{(4)}p_0}{5!},\\q_3&=\frac{2s^2\mathrm{D}_s^{(2)}p_2}{3!}-\frac{4s^4\mathrm{D}_s^{(4)}p_1}{5!}+\frac{6s^6\mathrm{D}_s^{(6)}p_0}{7!},\\q_n&=\sum_{k=1}^{n}(-1)^{k+1}\frac{2k}{(2k+1)!}s^{2k}\mathrm{D}_s^{(2k)}p_{n-k}.\end{aligned}\tag{4.3}$$

Then the series in β for the dynamic boundary condition becomes

$$r_0(s)+\beta r_1(s)+\beta^2 r_2(s)+\beta^3 r_3(s)+\cdots=\sum_{n=0}^{\infty}\beta^n r_n(s)=0,\tag{4.4}$$

where

$$r_0=2(s-1)/F^2+q_0^2-1,\tag{4.5}$$

$$r_n = \sum_{k=0}^{n} q_k q_{n-k} + 2K(s) \sum_{k=0}^{n-1} q_k q_{n-k-1}, \quad n = 1, 2, 3, \ldots . \tag{4.6}$$

This exact series form of the dynamic boundary condition is an infinite-order nonlinear differential equation for K that depends on s and four parameters: α, β, Ω, and F. Thus the uniform-vorticity solitary wave is a single-degree-of-freedom Hamiltonian system.

Consider the Boussinesq–Rayleigh approximation of (4.4) up to $O(\beta^2)$

$$2\frac{s-1}{F^2} + \frac{\Omega^2}{2}\left(\frac{s^2}{2} + \frac{1}{2s^2} - 1\right) + (\Omega + 1)\left(\frac{1}{s^2} - 1\right) + \beta\left\{\frac{\mathrm{d}K}{\mathrm{d}s}\left[\frac{\Omega^2}{3}\left(\frac{s^3}{2} + \frac{1}{2s} - s\right)\right.\right.$$
$$\left. + \frac{2\Omega}{3}\left(\frac{1}{2s} - s\right) + \frac{2}{3s}\right] + K\left[\Omega^2\left(\frac{s^2}{2} - \frac{1}{3} - \frac{1}{6s^2}\right) - \frac{2\Omega}{3}\left(1 + \frac{1}{s^2}\right) - \frac{2}{3s^2}\right]\Bigg\} = 0, \tag{4.7}$$

which is the exact nonlinear differential equation and permits integration in elementary functions. Integrating (4.7) with the boundary condition $K(1) = 0$ that corresponds to the equilibrium point $s = 1$, we obtain the Hamiltonian of the solitary wave,

$$H = \frac{1}{2}\left(\frac{\mathrm{d}s}{\mathrm{d}X}\right)^2 - \frac{(s-1)^2\left[12(1+\Omega)F^2 - 12s - F^2\Omega^2(s+3)(s-1)\right]}{2\beta F^2\left[\Omega(s^2-1) - 2\right]^2} = 0, \tag{4.8}$$

where the rational $\Pi(s)$ is the quotient of the polynomials in s of the fourth degree. For $\Omega = 0$, $\Pi(s)$ becomes a polynomial in s of the third degree and coincides with that by Lamb (1932, § 252).

For further analysis, it is convenient to introduce a new variable $q = s - 1$ representing the free surface in a moving frame of reference located at the far-upstream elevation. The anisotropic influence of vorticity of the primary flow results in two characteristic forms of the Hamiltonian of the vortical solitary wave on the stream with uniform vorticity. When vorticity is positive, the Hamiltonian is

$$H_p = \frac{1}{2}\left(\frac{\mathrm{d}q}{\mathrm{d}X}\right)^2 - \frac{q^2(\alpha - q)(q + q_3)}{2\beta(q - q_1)^2(q + q_1 + 2)^2}, \tag{4.9}$$

where $q_1 = (1 + 2/\Omega)^{1/2} - 1$, $q_3 = 4 + \alpha + 12/(\Omega F)^2$

$$\alpha = \{1 + 3/\Omega + 3[1 + 1/F^2 + 3/(\Omega^2 F^4)]/\Omega^2\}^{1/2} - 6/(\Omega F)^2 - 2. \tag{4.10}$$

Here $0 \leqslant q \leqslant \alpha < q_1$ and the denominator of the Hamiltonian has two real zeros. If vorticity is negative, the Hamiltonian takes the following form:

$$H_n = \frac{1}{2}\left(\frac{\mathrm{d}q}{\mathrm{d}X}\right)^2 - \frac{q^2(\alpha - q)(q + q_3)}{2\beta[(1+q)^2 + q_2^2]}, \tag{4.11}$$

where $q_2 = (-2/\Omega - 1)^{1/2}$. Here, the denominator possesses two complex-valued zeros. Solving (4.10) for F^2, we obtain the relationship between the Froude number and the amplitude,

$$F^2 = \frac{1 + \alpha}{1 + \Omega - (1 + \alpha/4)\alpha\Omega^2/3}, \tag{4.12}$$

which reduces to the well-known relationship $F^2 = 1 + \alpha$ for the irrotational solitary wave and agrees for small Ω with the results found by Benjamin (1962, equation (46))

and Miroshnikov (1996, equation (4.3)) on the basis of weakly nonlinear theory. Note that the local Froude number does not depend on the shallowness parameter.

In figure 3, we present four-dimensional Hamiltonian maps of the vortical solitary wave which are generalizations of two-dimensional and three-dimensional maps considered by Kolesnikov & Miroshnikov (1992) and Miroshnikov (1996), respectively. In agreement with (2.9), the phase motion of the Hamiltonian system is analogous to the motion of a particle in the gravity field, as the higher the potential energy of the system the lower the kinetic energy. Qualitatively finding three-dimensional trajectories of a particle in the potential well and projecting them on the two-dimensional plane of hydrodynamic variables, one, in fact, proves an existence theorem and finds the number and type of possible solutions; this is a non-trivial problem in nonlinear cases. So the four-dimensional Hamiltonian map could be regarded as an analog computer for the qualitative integration of (4.8).

The phase potential energy of the rotational solitary wave strongly depends on the Froude number. To find a first critical value of the Froude number corresponding to the emergence of the solitary wave, we solve the equation $\alpha = 0$ for F^2. The result,

$$F_1^2 = 1/(1+\Omega), \tag{4.13}$$

coincides with the critical value for the irrotational solitary wave, $F_{1i} = 1$, when $\Omega = 0$. In the first subcritical regime for $F < F_1$, the phase well has a local minimum at the initial point of the phase trajectory. Then the unique stable trajectory admissible by the far upstream condition is the straight line. The width and the depth of the well approach zero as F approaches F_1 from the left and the phase motion becomes unstable in the first critical regime for $F = F_1$. In the first supercritical regime for $F > F_1$, the phase well has a local maximum at the initial point of the phase trajectory. Then three trajectories may be displayed. The unbounded one corresponding to the cosech^2-solution for the irrotational solitary wave describes a solution blocking the upstream flow and contradicts the mass conservation law. The second trajectory resulting in a flat free surface is obviously unstable. Finally, the bounded trajectory of the rotational solitary wave coinciding with the sech^2-solution in the irrotational case starts and terminates at the potential barrier as the energy level of the system is equal to the height of the potential barrier.

The horizontal velocity of the solitary-wave stream beneath the crest readily follows from (2.2*a*) and (3.9) as the free-surface elevation is known, $s(0) = 1+\alpha$. In figure 4(*a*), increasing Ω reverses the flow in a neighbourhood of the crest. This flow separation starts when the horizontal velocity vanishes on the crest. It can be shown that this condition combined with (4.12) yields a second critical value of the Froude number for the formation of a single eddy near the crest,

$$F_{2p}^2 = \frac{1}{2}\frac{\alpha(5\alpha^2+22\alpha+20)^2}{10\alpha^4+79\alpha^3+232\alpha^2+288\alpha+128-2(1+\alpha)(2+\alpha)[3(5\alpha^2+12\alpha+8)]^{1/2}}. \tag{4.14}$$

Similarly, decreasing Ω shown in figure 4(*b*) forms a recirculating flow in a neighbourhood of the bottom. The flow separation now initiates when the horizontal velocity vanishes on the bottom. This condition and (4.12) yield a second critical value of the Froude number for the formation of a single eddy near the bottom,

$$F_{2n}^2 = \frac{1}{2}\frac{\alpha(11\alpha^3+46\alpha^2+68\alpha+48)^2(5\alpha^2+16\alpha+16)^{-1}}{11\alpha^4+46\alpha^3+74\alpha^2+48\alpha+24-2(1+\alpha)[3(11\alpha^2+24\alpha+12)(\alpha^2+4)]^{1/2}}. \tag{4.15}$$

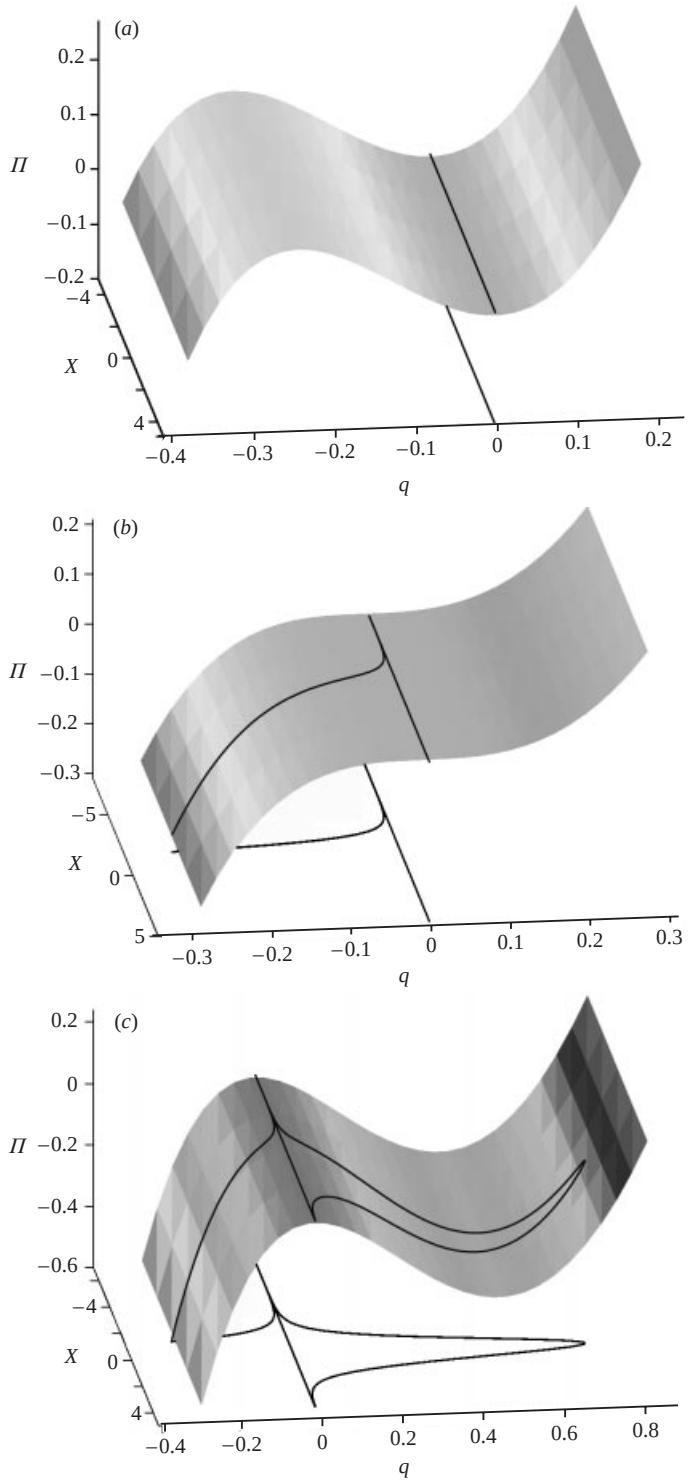

FIGURE 3. The four-dimensional Hamiltonian maps for $\beta = 0.1$ and $\Omega = -0.3$: (*a*) $F = 0.95 < F_1$; (*b*) $F = F_1 = 1.1952$; (*c*) $F = 1.6 > F_1$. Values of H are shown by shading.

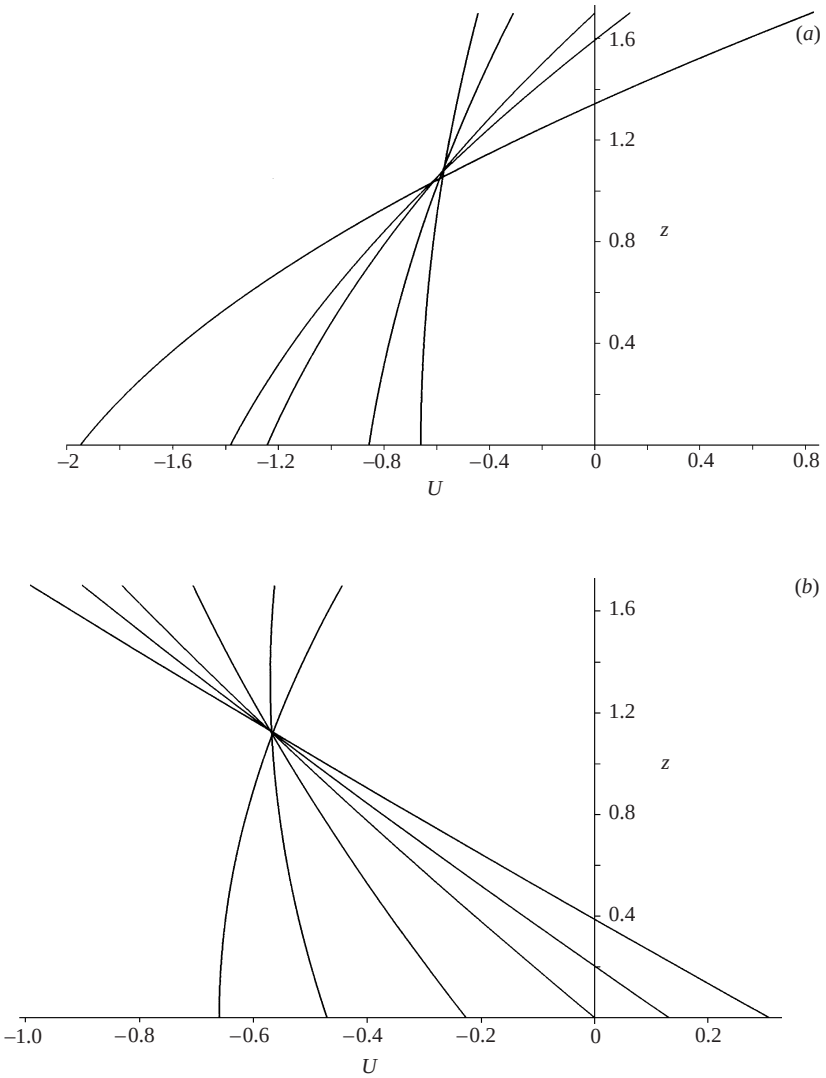

FIGURE 4. Velocity profiles for $\alpha = 0.7$ and $X = 0$. From right to left:
(*a*) $\Omega = 0.75, 0.5, 0.4163, 0.15, 0$; (*b*) $\Omega = -0.8, -0.65, -0.5393, -0.35, -0.15, 0$.

Thus the formation of recirculating flow depends only on α and the flow separation occurs if α is high enough.

Figure 5 displays the anisotropic effect of the upstream vorticity on an extreme amplitude of the solitary wave. For $\Omega > 0$, $\Pi(q)$ has a vertical asymptote at $q = q_1$ and increasing F deforms a nearly symmetric well into a highly asymmetric well. As α approaches q_1 from the left, the depth of the phase well becomes unbounded, resulting in a sharp-crested solitary wave. Solving the equation $\alpha = q_1$, we get a fourth critical value of the Froude number for the formation of the limiting configuration,

$$F_{4p}^2 = 6\frac{(\Omega + 3)(1 + \Omega/2)^{1/2} + \Omega}{8\Omega^2 + 21\Omega + 18}. \tag{4.16}$$

This topological mechanism of the generation of the corner flow greatly differs from

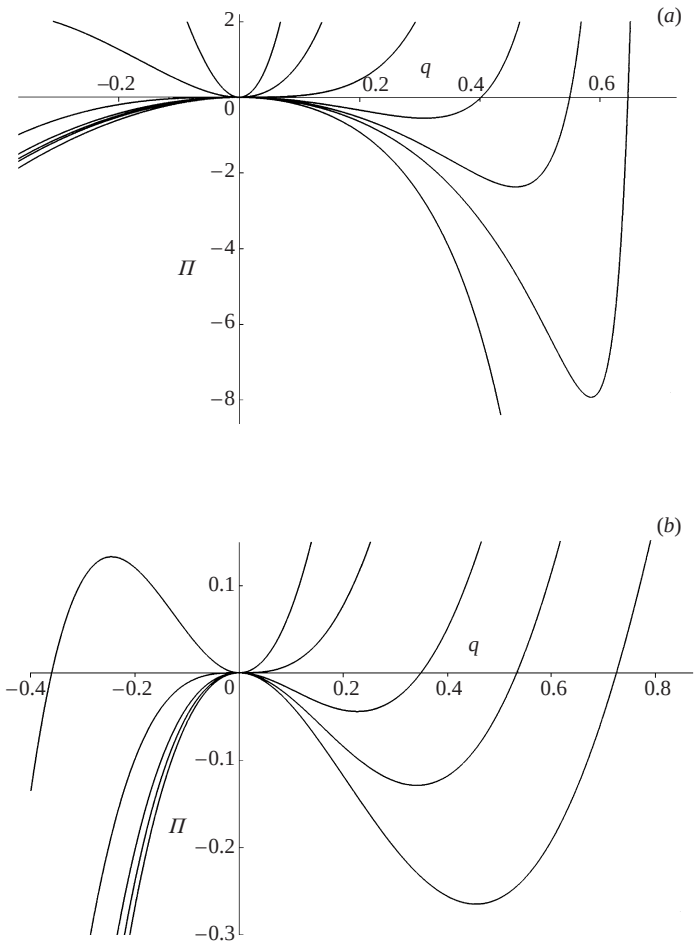

FIGURE 5. Cross-sections of the four-dimensional Hamiltonian maps for $\beta = 0.1$: (a) $\Omega = 1$, $q_1 = 0.7321$, $F_1 = 0.7071$, $F_{4p} = 1.006$, and from left to right $F = 0.2$, 4, 0.7071, 0.87, 0.93, 0.97, 1.006; (b) $\Omega = -0.3$ and from left to right $F = 0.95$, 1.1952, 1.4, 1.5, 1.6.

the mechanism of the Stock's corner flow that is generated by gravity, described by the dynamic boundary condition (2.17), and results in $F_{4S}^2 = 2\alpha$ (Vanden-Broeck 1994). The hydrodynamic implementation of this topological mechanism is discussed in § 5. The vertical asymptote does not exist for $\Omega \leqslant 0$ and the extreme wave is not bounded by the topological mechanism, as increasing F results in an unbounded width of the well shown in figure 5(b).

Figure 6(a) displays $F = F(\alpha, \Omega)$ given by (4.12) and all critical values of the Froude number of the rotational solitary wave, where $F_1 \leqslant F \leqslant F_4$, F_3 is a third critical value of the Froude number for the pressure instability calculated in § 6. We observe that the speed of the solitary wave increases with the growth of the wave amplitude and diminishes with the growth of the vorticity. F_{2p} approaches F_{4S} as α approaches zero. The difference between F_{2p} and F_{4S} does not exceed 8% for $\alpha \leqslant 2$. It is shown by the exact topological solution in the Appendix that, for fixed α, $F_{4S} \geqslant F_{2p} \geqslant F_{4p}$ when $\alpha \geqslant \alpha_B$.

To compare (4.12) with the weakly nonlinear theory by Benjamin (1962) and the numeric simulations by Vanden-Broeck (1994), curves are plotted in figure 6(b) in variables α and $G = 1/F^2$, where G is the dimensionless gravity. Expanding (4.12) up

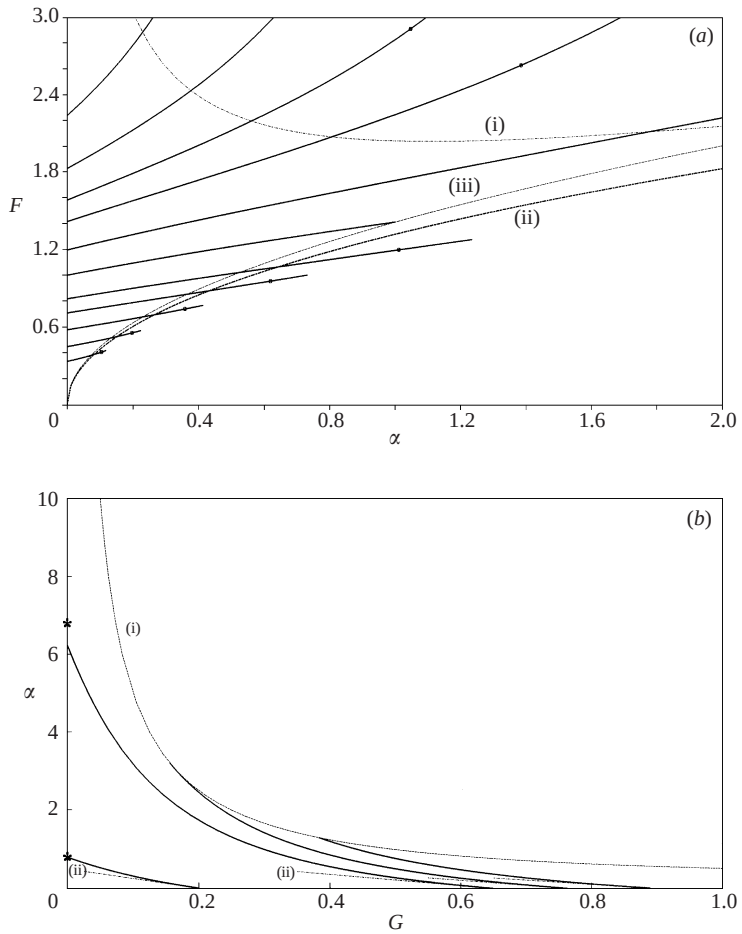

FIGURE 6. (*a*) F versus α for various values of Ω. The solid curves from top to bottom correspond to $\Omega = -0.8, -0.7, -0.6, -0.5, -0.3, 0, 0.5, 1, 2, 4, 8$. The curves terminate if $F = F_{4p}$ or $F = F_{4n}$. F_{2n} is shown by the dashed-dotted curve (i), F_{2p} by the bold dashed curve (ii), F_{4S} by the dashed curve (iii), F_{3n} and F_{3p} by points. (*b*) α versus G for various values of Ω. The solid curves from left to right correspond to $\Omega = -0.8, -0.35, -0.2364, -0.11$. The dashed curve (i) corresponds to F_{4S}, the asterisks to numeric simulations by Vanden-Broeck (1994), the dashed-dotted lines (ii) to the weakly nonlinear theory by Benjamin (1962).

to $O(\alpha^2)$, we obtain

$$G = 1 + \Omega - (1 + \Omega + \Omega^2/3)\alpha. \tag{4.17}$$

Equation (4.17) coincides with the asymptotic solution by Benjamin (1962) shown by dotted lines. In agreement with Vanden-Broeck (1994), there is an interval $\Omega_c \approx -0.2364 \leqslant \Omega \leqslant 0$, where the extreme amplitude is bounded by gravity, i.e. $F_{4n} = F_{4S}$. This relation corresponds to the dashed curves in figure 6. For $\Omega < \Omega_c$, the limiting configuration is not bounded by gravity and the branches of (4.12) extend for unbounded values of α without intersecting the broken line. The solitary wave on the stream with constant vorticity exists in conditions of weightlessness. For $G = 0$, the discrepancy between the current theory and the numerical simulations shown in figure 6(*b*) by asterisks is negligible within the graphical accuracy for $\alpha \leqslant 0.8$ and does not exceed 7% for $\alpha \leqslant 6$.

The main advantages of the Hamiltonian approach applied systematically in the present paper are the following: (i) the Hamiltonian of the vortical solitary wave permits the complete qualitative integration of the nonlinear dynamic problem by the four-dimensional Hamiltonian maps, and (ii) the Hamiltonian enables one to find the critical values of the Froude number connected with the vertical structure of the solitary-wave flow. In the next section, we consider the quantitative integration of the Hamiltonian that displays the horizontal structure of the uniform-vorticity solitary wave.

5. Flow structure

Integrating (4.8) written in terms of q with the boundary condition $X(\alpha) = 0$, we find the parametric solution for the solitary wave on the stream with constant vorticity

$$X = \mp\left[\frac{\beta(1+\alpha)}{3}\right]^{1/2}\left\{\frac{\Omega}{2\alpha^{1/2}}\left(4-\frac{b}{a}+\alpha\right)\arctan\left[\frac{a(\alpha-q)}{aq+b}\right]^{1/2}\right.$$
$$\left.+\frac{2}{(\alpha b)^{1/2}}\ln\frac{[b(\alpha-q)]^{1/2}+[\alpha(aq+b)]^{1/2}}{[q(b+\alpha a)]^{1/2}}-\frac{\Omega}{2}\frac{[(\alpha-q)(aq+b)]^{1/2}}{a}\right\}, \tag{5.1}$$

$$a = \Omega^2(1+\alpha)/12, \quad b = 1+\Omega+\Omega^2(4+\alpha)/12, \tag{5.2}$$

where minus and plus signs correspond to positive and negatives values of X, respectively. As $\Omega \to 0$, (5.1)–(5.2) may be expressed in the explicit form coinciding with that by Lamb (1932, § 252, equation (12)). For $\Omega = -\beta\delta_0$, the free-surface profile reduces to that by Miroshnikov (1996, equation (3.21)) with $\delta_1 = 0$. Free-surface profiles are shown in figure 7 for comparable amplitudes and several values of Ω. The uniform vorticity strongly affects an effective wavelength of the solitary wave. Comparing with the irrotational solitary wave shown in figure 7(b), we observe that the rotational wave is nearly half the length for $\Omega = 2$ and is one and half times longer for $\Omega = -0.8$. As F approaches F_{4p} from the left, the profile approaches the sharp-crested limiting configuration in figure 7(a).

Reducing (3.9) up to $O(\beta^2)$ by (4.8) in q, we obtain the stream function as a cubic polynomial in z

$$\Psi = a_3 z^3 + a_2 z^2 + a_1 z, \tag{5.3}$$

where a_1, a_2 and a_3 are rational functions of q, α and Ω:

$$a_3 = \frac{q}{24a_4(1+q)^2}\{q^2[\Omega^2 a(4+a)-12(1+\Omega)]+q[\Omega^2(12+8a-a^2)$$
$$\times 12(\Omega+1)(2a+3)]-2\Omega^2 a(4+a)-24\Omega(1+a)\},$$
$$a_4 = (1+q)(1+\alpha)(\Omega q^2+2\Omega q-2), \quad a_2 = -\Omega/2,$$
$$a_1 = \frac{1}{24a_4}\{12q^4\Omega^2(1+\alpha)-q^3[\Omega^2(\alpha^2-44\alpha-48)-12(1+\Omega)]$$
$$+q^2[\Omega^2(\alpha^2+64\alpha+60)-12(\Omega+1)(2\alpha+3)]+q[2\Omega^2(\alpha^2+28\alpha+24)$$
$$+24\Omega(1+\alpha)]-48(\Omega+1)(\alpha+1)\}.$$

Figures 8(b) and 8(c) show the single-valued streamlines with fixed α and β in the second subcritical regime for $F_1 < F < F_{2n}$ and the second critical regime for $F = F_{2n}$, respectively. Corresponding streamlines of the irrotational solitary wave are given in figure 8(a) for comparison. Note that the stagnation zone is formed near the bottom

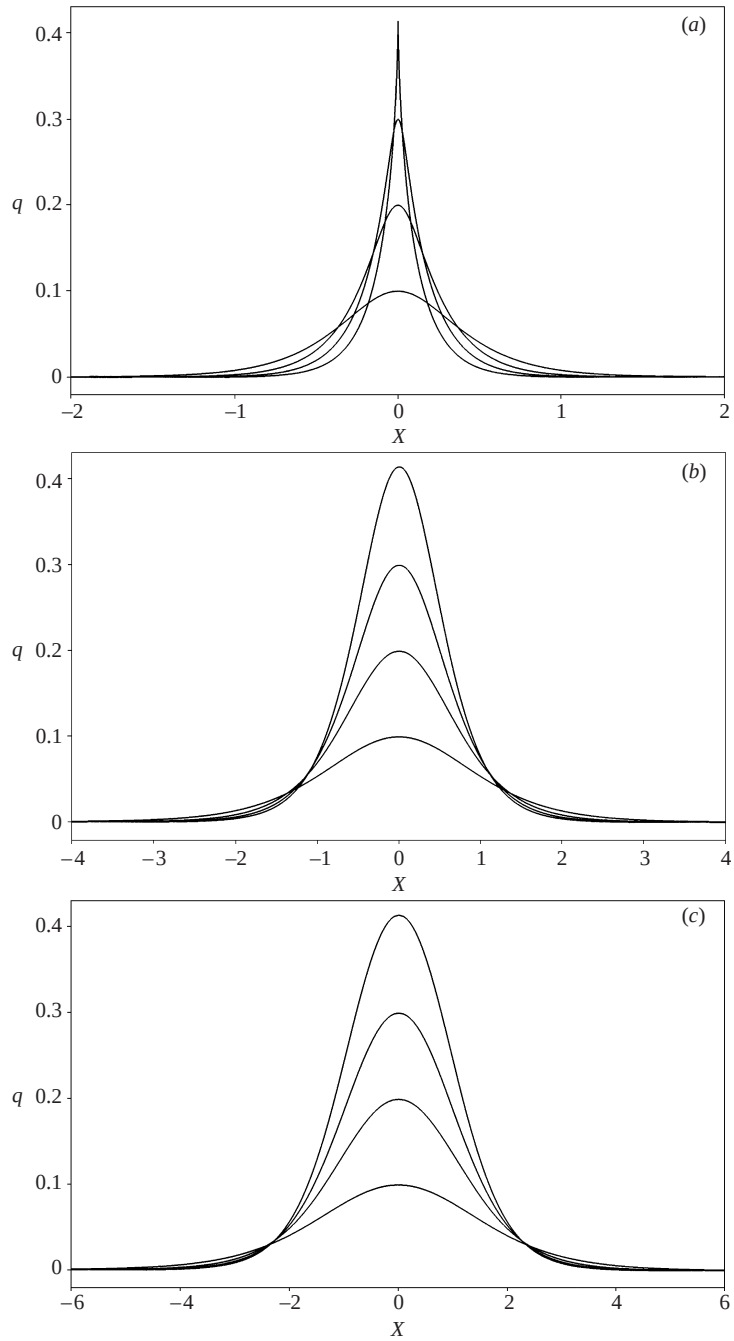

FIGURE 7. Free-surface profiles for $\beta = 0.1$: (*a*) $\Omega = 2$, and from bottom to top $\alpha = 0.1, 0.2, 0.3, 0.4142$; (*b*) $\Omega = 0$, $\alpha = 0.1, 0.2, 0.3, 0.4$; (*c*) $\Omega = -0.8$, $\alpha = 0.1, 0.2, 0.3, 0.4$.

in the second critical regime for the negative shear. The flow separation near the bottom in the second supercritical regime for $F_{2n} < F < F_{4n}$ is shown in figure 8(*d*).

Besides the bifurcating bottom streamline, figure 8(*d*) presents double-valued streamlines of the recirculating flow. The upper $l_t = l_t(q, \alpha, \Omega)$ and lower $l_b = l_b(q, \alpha, \Omega)$

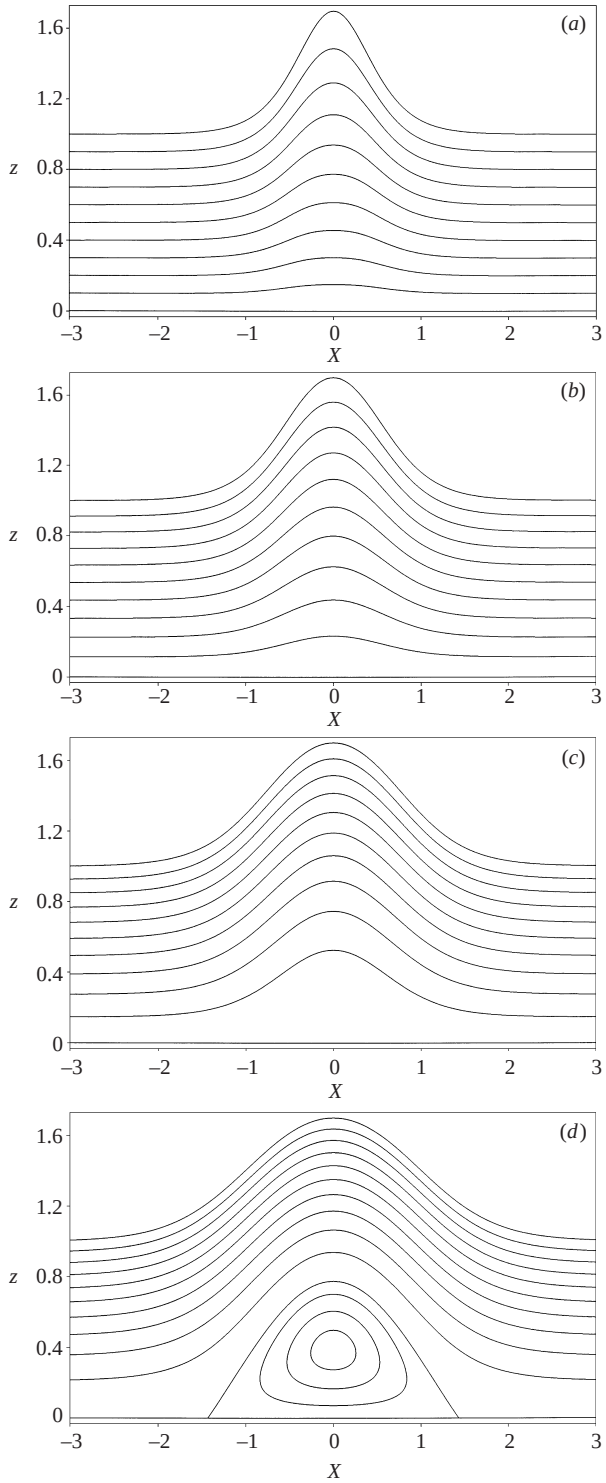

FIGURE 8. Streamlines for $\alpha = 0.7$, $\beta = 0.1$, and (*a*) $\Omega = 0$, (*b*) $\Omega = -0.25$, (*c*) $\Omega = -0.5393$, (*d*) $\Omega = -0.8$. From bottom to top (*a–c*) $\Psi = (1 + \Omega/2)n/10$, $n = 0, 1, \ldots, 10$; (*d*) $\Psi = -0.02$, -0.04, -0.054, $(1 + \Omega/2)n/10$, $n = 0, 1, \ldots, 10$.

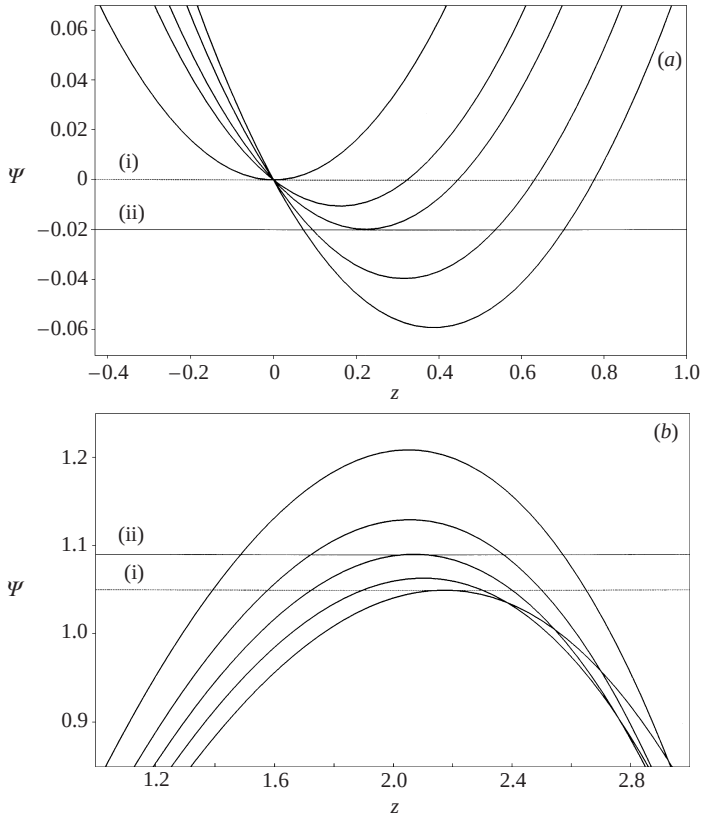

FIGURE 9. (*a*) Plot of Ψ as a function of z for the solitary-wave flow with $\Omega = -0.8$, $\alpha = 0.7$, and from left to right $q = 0.22$, 0.4, 0.48, 0.6, 0.7; the dotted line (i) corresponds to $\Psi = 0$, the solid line (ii) to $\Psi = -0.02$. (*b*) Plot of Ψ as a function of z for the solitary-wave flow with $\Omega = 0.1$, $\alpha = 1.65$, and from left to right $q = 1.65$, 1.5, 1.4, 1.3, 1.17; the dotted line (i) corresponds to $\Psi = 1.05$, the solid line (ii) to $\Psi = 1.09$.

recirculating streamlines are shown in figure 9(*a*) as points of intersection of curves for Ψ with a horizontal line $\Psi = -0.02$. The bifurcation starts at a point $z_{lb} = z_{lb}(q, \alpha, \Omega)$ of a local minimum of $\Psi = \Psi(z)$, where the branches l_t and l_b merge. Cubic curves for Ψ in figure 9(*a*) have two points of intersection with horizontal lines $\Psi = \Psi_0$ on the interval $0 \leqslant z \leqslant 1 + \alpha$. Calculations of the centre of the separated eddy $z_{cb} = z_{lb}(\alpha, \alpha, \Omega)$ and a minimal value of the stream function $\Psi_{\min} = \Psi(z_{cb})$ complete the problem, where $\Psi_{\min}$ determines the flux of the recirculating flow. The single-eddy bifurcation looks like a merged pair of direct and reversed pitchfork bifurcations due to the symmetry of the solitary-wave problem. As the steady recirculating flow may be replaced with a bottom topography $z = i_b$, the solution of the kinematic problem considered is equivalent to the solution for a steady flow over a streamlined bump. For the periodic waves, the corresponding eddy formed by the flow separation near the bottom was obtained in the numeric simulations by Teles da Silva & Peregrine (1988).

Figures 10(*a*) and 10(*b*) show the effect of the positive shear with fixed α and β in the second subcritical regime for $F_1 < F < F_{2p}$ and the second critical regime for $F = F_{2p}$, respectively. In the critical regime, the stagnation zone is now formed in the neighbourhood of the crest. The single eddy separated near the crest is presented

in figure 10(c) in the second supercritical regime for $F_{2p} < F < F_{4p}$. Figure 9(b) shows l_t and l_b as points of intersection of curves for Ψ with a horizontal line $\Psi = 1.09$. The bifurcation starts at a point $z_{ls} = z_{ls}(q, \alpha, \Omega)$ of a local maximum of $\Psi = \Psi(z)$ that is the point of merging l_t and l_b. Cubic curves for Ψ have two points of intersection with horizontal lines $\Psi = \Psi_0$ as a third point of intersection lies outside the interval $0 \leqslant z \leqslant 1 + \alpha$ for $q > q_{ls}$. Calculating z_{ls} beneath the wave crest and the corresponding value of the stream function, we find the vertical coordinate of the centre of the separated eddy $z_{cs} = z_{ls}(\alpha, \alpha, \Omega)$ located at $X = 0$ and its flux $\Psi_{\max} = \Psi(z_{cs})$. For $\Omega = O(\beta)$, the eddy generated by the flow separation near the crest was obtained in the framework of the weakly nonlinear theory by Miroshnikov (1995, 1996).

Figure 10(d) presents the nearly critical regime for $F \to F_{4p}$ that results in blocking of the upstream flow by the growing eddy because its height approaches $1 + \alpha$ as F approaches F_{4p}. Replacing the recirculating flow with a surface bluff topography $z = i_s$, we see that the limiting configuration corresponds to the flow blocking by a barrier which looks like a knife. Similarly, the flow show in figure 10(c) may be treated as a free-surface flow generated by a moving immersed streamlined body with the shape given by $z = i_s$.

The typical feature of the coherent-wave–vortex structures shown in figures 10(c), 10(d), 11(c) and 11(d) is the double-corner flow with unclosed streamlines that corresponds to the Stock's single-corner flow for the extreme waves; this is because, in both cases, the maximal elevation of a fluid particle on the free surface of a wavy domain is restricted by gravity. In the Appendix, it is shown that the exact value of the corner angle of the coherent-wave–vortex structure is equal to that of the extreme wave. The corner angle, θ, of the double-corner flow in the Boussinesq–Rayleigh approximation deviates somewhat from $\theta_S = 120^\circ$ if $\alpha - \alpha_B$ is small enough. For example, $\theta = 111.7^\circ$, $(\theta - \theta_S)/\theta_S = 7\%$ for $\Omega = 0.1$, $\beta = 0.1$, $\alpha = 1.12$ and $\theta = 120.5^\circ$, $(\theta - \theta_S)/\theta_S = 0.4\%$ for $\Omega = 0.42$, $\beta = 0.1$, $\alpha = 0.7$. A similar conclusion holds for the single-corner flow corresponding to the topological limiting structure. For example, $\theta = 132.1^\circ$, $(\theta - \theta_S)/\theta_S = 10\%$ for $\Omega = 0.95$, $\beta = 0.1$, $\alpha = 0.7$.

Figures 11(a), 11(b), 11(c) and 11(d) show the flow separation with fixed vorticity and various α in the second subcritical regime for $F_1 < F < F_{2p}$, the second critical regime for $F = F_{2p}$, and the second supercritical regime for $F_{2p} < F < F_{3p}$, respectively. This set of figures displays that the flow separation in steep rotational solitary waves is a typical nonlinear threshold effect. The results obtained agree with a theorem by Batchelor (1956) that steady laminar flows with closed streamlines have a uniform vorticity distribution at high Reynolds numbers. In figures 11(a) and 11(b), the shear flow pattern of the vortical solitary wave is formed by the unclosed streamlines, similar to the streamlines of the irrotational wave that are always unclosed. In figures 11(c) and 11(d), the flow pattern of the resulting coherent wave–vortex structure is divided into two domains. The first domain is the two sharp-crested wavy domain with the unclosed streamlines, the upper border $z = 1 + q$ for $0 \leqslant q \leqslant q_s$ and $z = i_s$ for $q_s \leqslant q \leqslant \alpha$. The second is the double-corner recirculating domain with closed streamlines, the upper border $z = 1 + q$, and the lower border $z = i_s$ for $q_s \leqslant q \leqslant \alpha$. In the theories of coherent structures, the solutions are formed by two stream functions for domains with closed and unclosed streamlines that are matched on separating streamlines (see reviews by Flierl 1987; Meleshko & van Heijst 1994; Chavanis & Sommeria 1998). The current flow pattern is given by the unique stream function (5.3) that may be thought of a surface $\Psi = \Psi(X, z)$ in the three-dimensional space (X, z, Ψ). Then figures 11(a)–11(d) are contour plots of Ψ, where the bifurcating closed

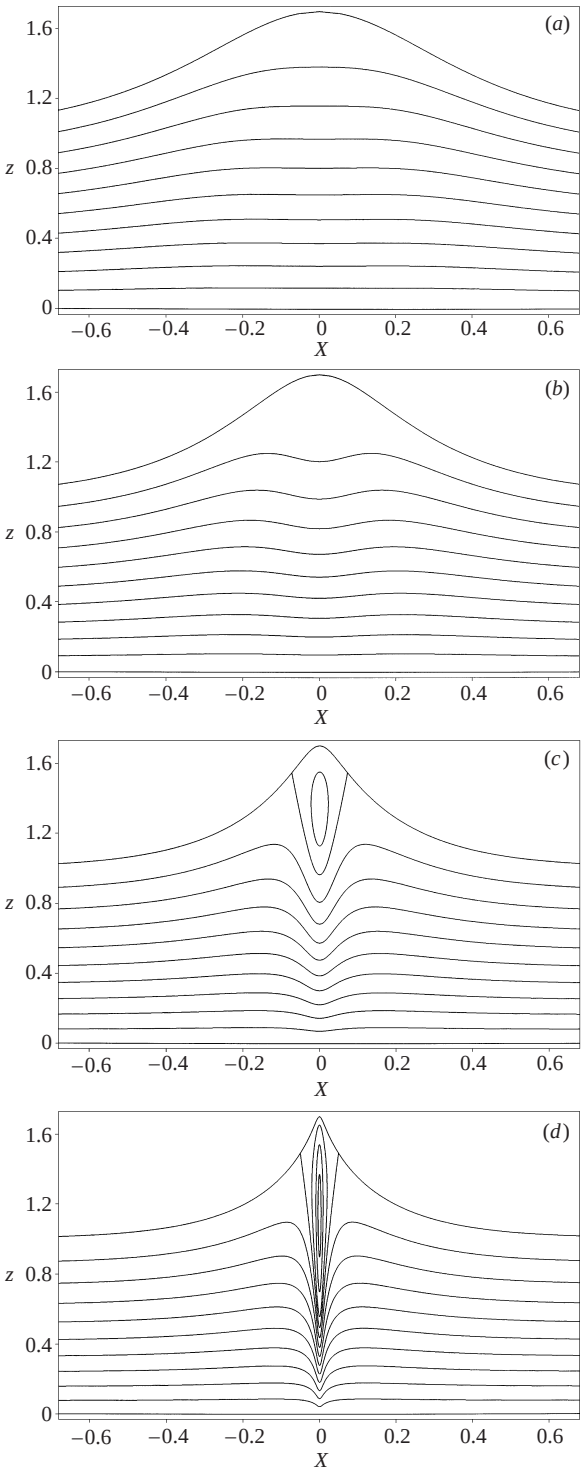

FIGURE 10. Streamlines for $\alpha = 0.7$, $\beta = 0.1$ and (a) $\Omega = 0.2$, (b) $\Omega = 0.4164$, (c) $\Omega = 0.75$, (d) $\Omega = 0.95$. From bottom to top $\Psi = (1 + \Omega/2)n/10$ and (a, b) $n = 0, 1, \ldots, 10$; (c) $n = 0, 1, \ldots, 10, 10.7$; (d) $n = 0, 1, \ldots, 10, 11, 13, 15$.

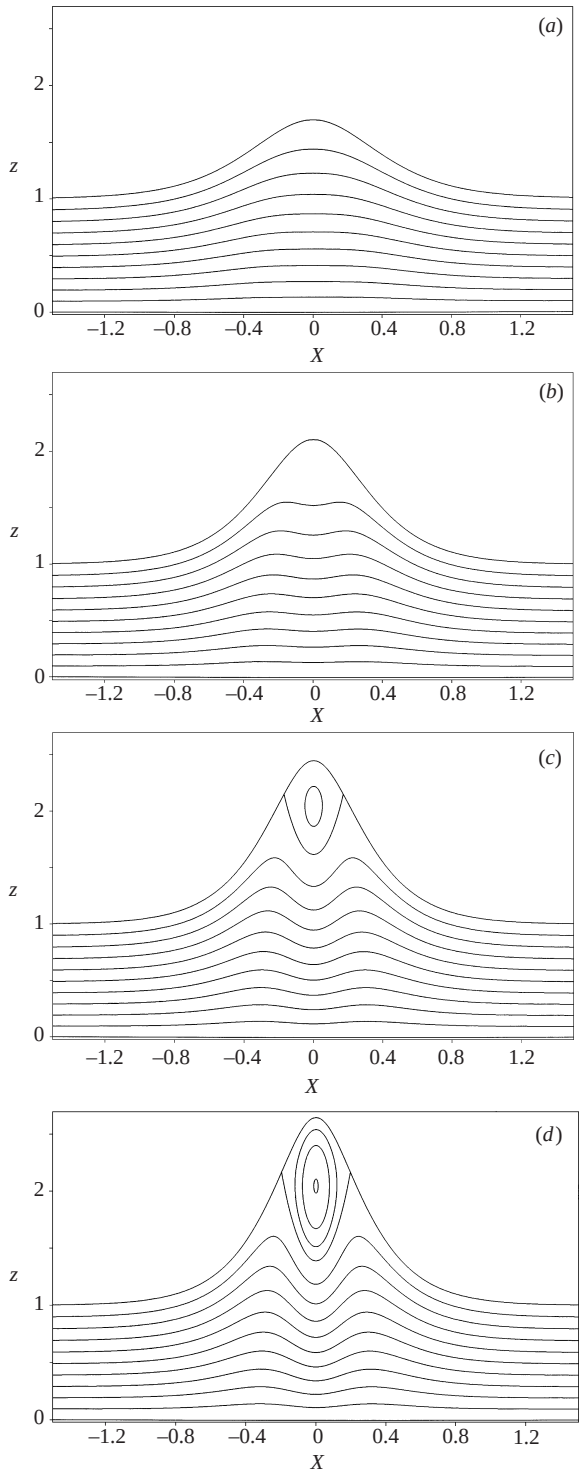

FIGURE 11. Streamlines for $\Omega = 0.1$, $\beta = 0.1$, and (a) $\alpha = 0.7$, (b) $\alpha = 1.11$, (c) $\alpha = 1.45$, (d) $\alpha = 1.65$. From bottom to top $\Psi = (1 + \Omega/2)n/10$ and (a, b) $n = 0, 1, \ldots, 10$; (c) $n = 0, 1, \ldots, 10, 10.5$; (d) $n = 0, 1, \ldots, 10, 10.5, 11, 11.5$.

streamlines correspond to cross-sections of the local maxima of Ψ and the single-valued unclosed streamlines to cross-sections of the global minima of Ψ. Hence all partial derivatives of Ψ are continuous on the separating streamlines as derivatives of the unique function. Any discontinuity of the derivatives of Ψ should be considered as an extra hydrodynamic effect (a point eddy, a point dipole, a vortex sheet, a point pressure source, etc.) that was not directly included in the primitive equations (Izrar & Lusseyran & Miroshnikov 1995). The continuity of the solution obtained for the solitary wave with the vortical core naturally results from the single-eddy bifurcation.

6. Pressure

The distribution of pressure (2.16) is determined by competition between three factors: gravity, inertia and vorticity. The dynamic boundary condition for the dimensionless pressure is that the pressure vanishes on the free surface, $P = 0$ on $z = 1 + q$. The far-upstream condition states that the pressure becomes hydrostatic at upstream infinity, $P = 1 + z$ for $q = 0$. Using (4.8) in terms of q and (5.3), we have

$$P(q, z) = \frac{(1 + q - z)(c_2 z^2 + c_1 z + c_0)}{4(q+1)^4[(\alpha\Omega^2(\alpha+4) - 12(\Omega+1)][\Omega q(q+2) - 2]}, \tag{6.1}$$

where c_2, c_1, c_0 are the fourth-degree, the sixth-degree, and the seventh-degree polynomials in q with coefficients depending on parameters α and Ω, respectively. In this paper, the analytic calculations were implemented using the symbolic manipulation package MAPLE available commercially. The final results of the symbolic calculations for streamlines and critical values of parameters were verified using numerical subroutines provided by MAPLE. (The files containing the symbolic and numeric calculations are available from the author upon request.)

Figure 12(a) displays the pressure profiles for the irrotational solitary wave as a function of X for several values of z because such a presentation may be compared with available field observations. The corresponding flow pattern is shown in figure 8(a). Pressure signatures of the wave have the same single-peaked shape as the streamlines. Similar single-peaked curves are obtained for pressure profiles in the second subcritical regime for $F_1 < F < F_{2n}$. In the second critical regime for $F = F_{2n}$, formation of the stagnation zone at the bottom in figure 8(c) results in flattening of the pressure profiles shown in figure 12(b). In the second supercritical regime for $F_{2n} < F < F_{3n}$, flow separation near the bottom is displayed by double-peaked pressure profiles shown in figure 12(c). This pressure drop is related to faster streaming near the free surface because of the blocking of the flow near the bottom by the separated eddy. Note that the pressure profile does not depend on z monotonically. In the third supercritical regime for $F_{3n} < F < F_{4n}$ presented in figure 12(d) corresponding to figure 8(d), the pressure drops below the atmospheric value resulting in a three-dimensional pressure instability which cannot be treated in the present two-dimensional theory. See Teles da Silva & Peregrine (1988) for the field image of a wave subjected to the pressure instability shown in their figure 18.

For $\Omega > 0$, figures 13(a), 13(b), 13(c) and 13(d) show the pressure profiles in the second subcritical regime for $F_1 < F < F_{2p}$, the second critical regime for $F = F_{2p}$, the third subcritical regime for $F_{2p} < F < F_{3p}$ and the third supercritical regime for $F_{3p} < F < F_{4p}$, respectively. The flow patterns corresponding to figures 13(a), 13(c) and 13(d) are presented in figures 10(a), 10(c) and 10(d). The effect of positive

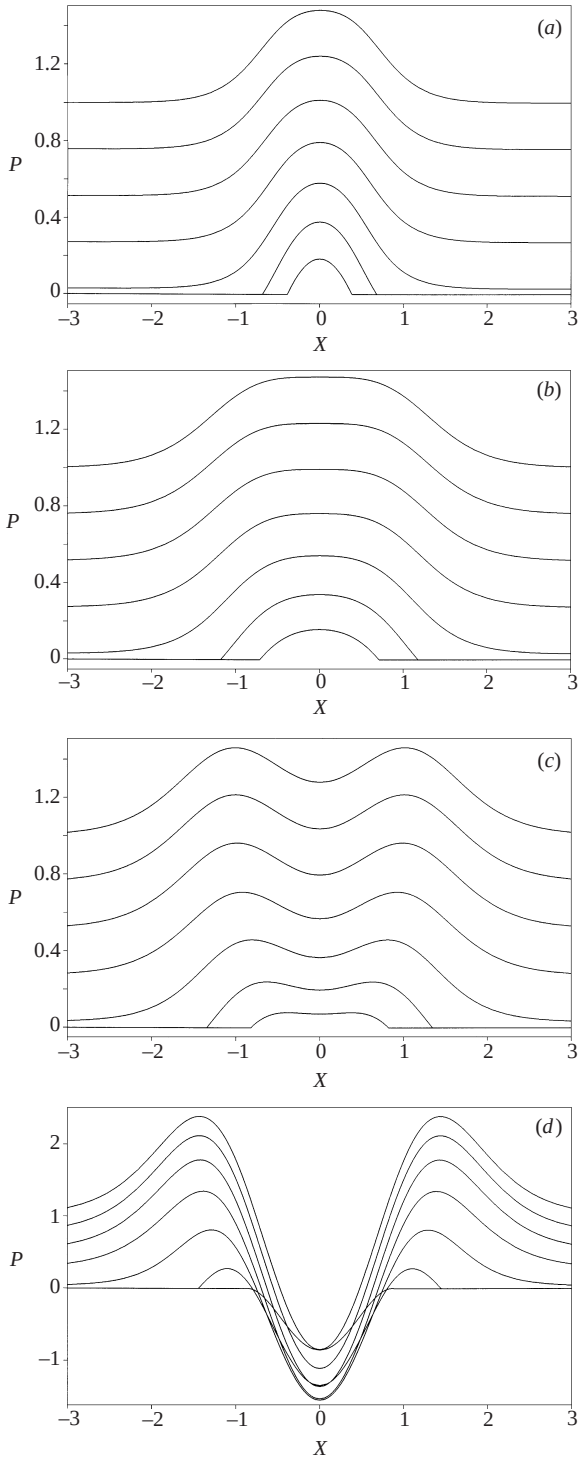

FIGURE 12. Pressure profiles for $\alpha = 0.7$, $\beta = 0.1$, and (*a*) $\Omega = -0.0001$, (*b*) $\Omega = -0.5393$, (*c*) $\Omega = -0.7$, (*d*) $\Omega = -0.8$. From top to bottom $z = (1 + \alpha)n/7$, $n = 0, 1, \ldots, 6$.

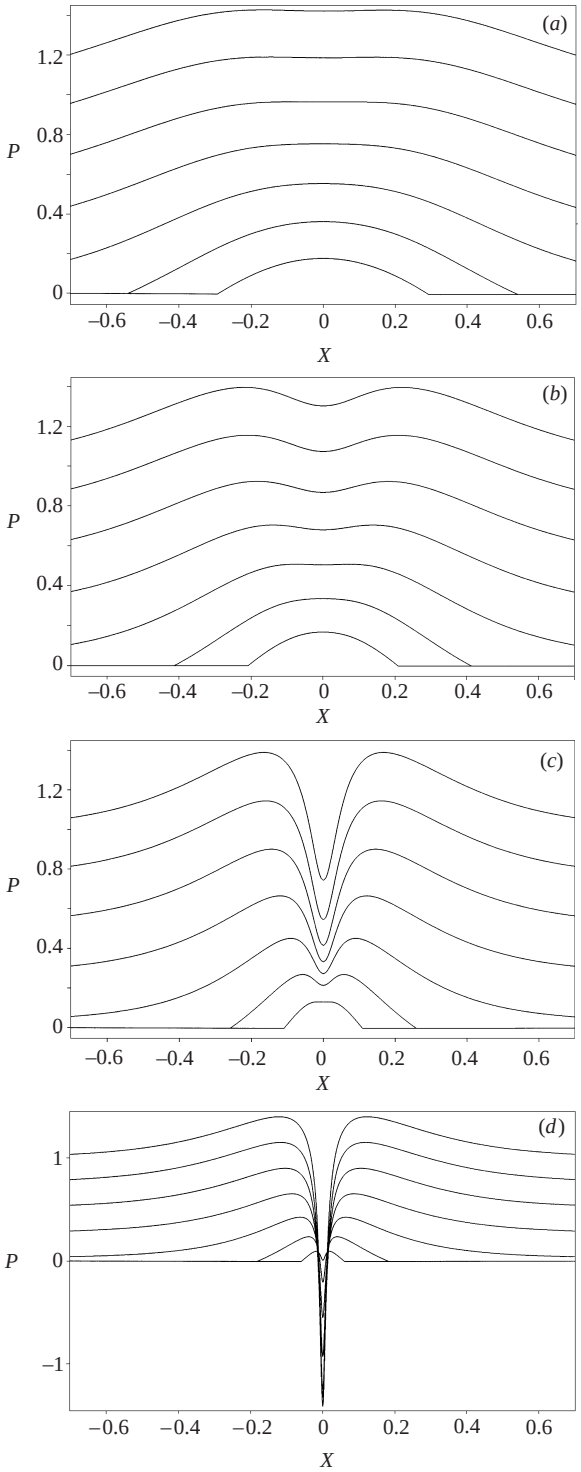

FIGURE 13. Pressure profiles for $\alpha = 0.7$, $\beta = 0.1$, and (*a*) $\Omega = 0.2$, (*b*) $\Omega = 0.4164$, (*c*) $\Omega = 0.75$, (*d*) $\Omega = 0.95$. From top to bottom $z = (1 + \alpha)n/7$, $n = 0, 1, \ldots, 6$.

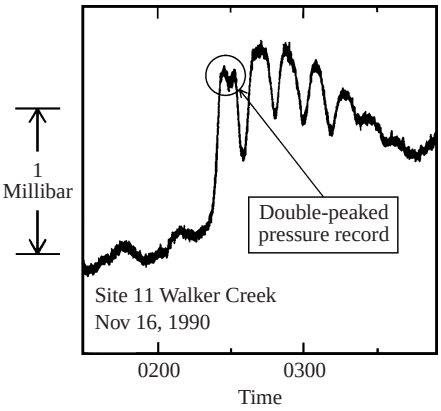

FIGURE 14. Observed double-peaked pressure record corresponding to the highest solitary wave of an amplitude-ordered family of atmospheric solitary waves. From Brown & Christie (1998).

vorticity is stronger than the effect of negative since the double-peaked pressure profile is displayed for $F = F_{2p}$. The pressure drops faster near the crest due to the separated eddy and results in the instability. The order of the value of the horizontal scale of the pressure drop generated by the flow separation is equal to the width of the eddy.

Solving $P'(\alpha, z) = 0$ with the given Ω for z, we find $z_{3n} = z_{3n}(\alpha)$ and $z_{3p} = z_{3p}(\alpha)$ for the negative and positive vorticity such that the pressure profile has a local minimum beneath the crest. Then critical values of α are solutions of $P(\alpha, z_{3n}) = 0$ and $P(\alpha, z_{3p}) = 0$, which were solved numerically, and critical values of F follow from (4.12). F_{3n} and F_{3p} are shown in figure 6(a) to display the third subcritical regimes for $F_{2n} < F < F_{3n}$ and $F_{2p} < F < F_{3p}$, where the coherent wave–vortex structures are stable both for negative and positive vorticity. In the third supercritical regime for $F > F_{3p}$, the atmospheric air puts pressure on the eddy and the rotational solitary wave breaks locally in the neighbourhood of the crest prior to formation of the limiting configuration. This local breaking is often observed for steep waves on a slightly inclined beach in field conditions.

Figure 14 shows the double-peaked pressure profile observed in a family of steep atmospheric solitary waves. This figure is reproduced from the study by Brown & Christie (1998) by the kind permission of those authors. Although the field observations were recorded for internal solitary waves, this qualitative comparison is an impressive indirect manifestation of stable coherent wave–vortex structures.

7. Conclusions

In this paper the extension of the Boussinesq–Rayleigh approximation to the interaction of the free-surface solitary wave and the shear shallow layer with constant vorticity is studied using a novel parameterized formulation of the kinematic and dynamic problems that admit an exact solution in terms of the single-eddy bifurcation which preserves continuity of all derivatives on separating streamlines. The resulting extreme wave–vortex structure is treated at the corner points of the wavy and vortical domains by the exact topological solution continuing the Stokes, Milne-Thompson (1968), and Delachenal (1973) solutions for the extreme waves.

It is shown that the uniform-vorticity solitary wave is a Hamiltonian system to any order of approximation. The detailed analysis of the four-dimensional Hamiltonian

maps reveals the threshold values of the dimensionless parameters for the following flow regimes: the emergence of the solitary wave, the flow separation near the crest, the flow separation near the bottom, and the formation of the topological extreme configuration. The results obtained show that the Bernoulli integral displays the double-peaked pressure profile indicating development of the coherent wave–vortex structure. Critical values of the dimensionless parameters for the pressure instability are calculated and it is shown that there is a certain interval of the Froude numbers where the solitary wave with the vortical core is stable both for negative and positive vorticity. The theoretical results are compared with previous weakly nonlinear theories, numerical simulations and field observations with satisfactory agreement.

The author is grateful to Dr Debra M. Szybinski for the helpful organization of the Summer 1999 Scholar-in-Residence Program at New York University. It is a pleasure to thank Professor David W. McLaughlin, Professor Esteban G. Tabak, Professor David M. Holland, and, especially, Professor Sylvain E. Cappell for being the author's hosts at the Courant Institute for Mathematical Sciences (NYU).

Appendix. Topological solution

Milne-Thompson (1968) and Delachenal (1973) showed that the sharp crest of the limiting form of a progressive rotational wave should have an angle of 120° and the vorticity only affects the curvature on each side. This theoretical result was confirmed by numeric simulations of solitary waves on water of finite depth with constant vorticity by Teles da Silva & Peregrine (1988) and Vanden-Broeck (1994).

To consider the limiting configuration and the single-eddy bifurcation in a small neighbourhood of corner points, we look for a topological solution in polar coordinates as shown in figures 15(*a*) and 15(*b*), respectively. The polar coordinates are given by

$$-X = r\cos\varphi, \quad 1 + \alpha_B - z = y = r\beta^{-1/2}\sin\varphi, \tag{A 1}$$

where α_B is the nonlinearity associated with the bifurcation point of the free-surface streamline; $\alpha_B = \alpha$ for the single-corner flow. Note that β is used to take shallow water into account. In the previous theories, $\beta = 1$. Transformation (A 1) diverges as $\beta \to 0$, which shows that the Stokes corner flow does not exist for vanishing β, in agreement with the Boussinesq–Rayleigh solution. Formulation of the topological problem is given by (2.3), the free-surface part of the kinematic condition (2.5), and (2.17) written in the polar coordinates

$$\frac{\partial^2\Psi}{\partial r^2} + \frac{1}{r}\frac{\partial\Psi}{\partial r} + \frac{1}{r^2}\frac{\partial^2\Psi}{\partial\varphi^2} = -\frac{\Omega}{\beta}, \tag{A 2}$$

$$y = 1 + \alpha_B - s(-r\cos\varphi), \quad \Psi = 1 + \frac{\Omega}{2}, \quad \beta\left[\left(\frac{\partial\Psi}{\partial r}\right)^2 + \frac{1}{r^2}\left(\frac{\partial\Psi}{\partial\varphi}\right)^2\right] + 2\frac{\alpha_B - y}{F^2} = 1. \tag{A 3}$$

We satisfy (A 2) and the kinematic boundary condition by

$$\Psi = 1 + \frac{\Omega}{2} - \frac{\Omega}{4\beta}r^2 + D_m r^m \sin m(\varphi - A) + C_n r^n \cos n(\varphi - B), \tag{A 4}$$

where the extra partial solution of the Laplace equation is added to Milne-Thomson's solution to satisfy the nonlinear dynamic boundary condition exactly. Here, n and

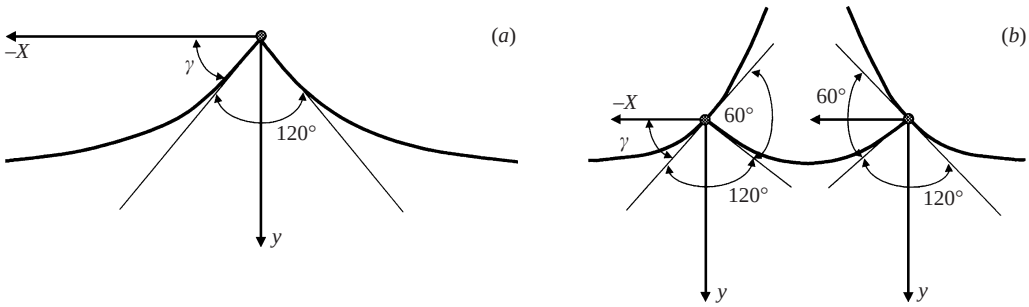

FIGURE 15. Polar coordinates for (*a*) the single-corner and (*b*) double-corner flow.

m are the smallest exponents of a power series in r since the velocity of the fluid is necessarily zero when $r = 0$. From (A 4) and (A 3) it follows that $m = 3/2$, $n = 2$,

$$F = (2\alpha_B)^{1/2}. \tag{A 5}$$

Equating to zero the coefficients of all powers of r, we obtain

$$r: \qquad \tfrac{9}{4}\beta D_m^2 - \frac{\sin\varphi}{\alpha_B \beta^{1/2}} = 0, \tag{A 6}$$

$$r^{3/2}: \qquad \tfrac{3}{2}D_m\Big\{4C_n[\sin\tfrac{3}{2}(\varphi - A)\cos 2(\varphi - B) - \cos\tfrac{3}{2}(\varphi - A)\sin 2(\varphi - B)] - \frac{\Omega}{\beta}\sin\tfrac{3}{2}(\varphi - A)\Big\} = 0, \tag{A 7}$$

$$r^2: \qquad \beta\left[\frac{\Omega^2}{4\beta^2} + 4C_n^2 - 2\frac{\Omega}{\beta}C_n\cos 2(\varphi - B)\right] = 0. \tag{A 8}$$

When $\Omega = 0$, $\alpha_B = \alpha$ and $C_n = 0$, (A 6) coincides with the equation for the Stokes corner flow. When $\alpha_B = \alpha$, $C_n = 0$ and terms $O(r^2)$ are neglected, (A 6)–(A 7) coincide with the relevant system by Milne-Thomson (1968, § 14.50, equation (7)) taking into account the different notation.

Equation (A 7) is always satisfied if $\sin 3(\varphi - A)/2 = 0$ and $\sin 2(\varphi - B) = 0$. In the case of the single-corner flow,

$$\left.\begin{array}{lll} A = \gamma, & B = \gamma, & \varphi = \gamma, \\ A = \gamma, & B = \gamma + 2\pi/3, & \varphi = \gamma + 2\pi/3, \end{array}\right\} \tag{A 9}$$

where symmetry of the rotational solitary wave means that $\gamma = \pi/6$,

$$C_n = \frac{\Omega}{4\beta}, \quad D_m = \frac{1}{3\beta^{3/4}}\left(\frac{2}{\alpha}\right)^{1/2}. \tag{A 10}$$

In the case of the double-corner flows, we get for the left-hand and right-hand bifurcation points, respectively,

$$\left.\begin{array}{lll} A = \gamma, & B = \gamma, & \varphi = \gamma, \\ A = \gamma, & B = \gamma + 2\pi/3, & \varphi = \gamma + 2\pi/3, \\ A = \gamma + \pi, & B = \gamma, & \varphi = \gamma + 2\pi/3 + \pi/3, \end{array}\right\} \tag{A 11}$$

$$\left.\begin{array}{lll} A=\gamma, & B=\gamma, & \varphi=\gamma, \\ A=\gamma, & B=\gamma+2\pi/3, & \varphi=\gamma+2\pi/3, \\ A=\gamma+5\pi/3, & B=\gamma, & \varphi=\gamma+2\pi/3+\pi, \end{array}\right\} \tag{A 12}$$

where $C_n = \pm\frac{1}{4}\Omega\beta^{-1}$, $D_m = \frac{2}{3}\alpha_B^{-1/2}\beta^{-3/4}\sin^{1/2}\varphi$. Thus the angle between the limiting branches of the wavy region is 120° and the angle between the double-valued branches of the recirculating zone is 60°. The above reasoning remains valid even if Ω is not constant but a bounded function of r, for we can replace Ω with the leading term of vorticity in the immediate neighbourhood of the bifurcation points.

REFERENCES

Batchelor, G. K. 1956 On steady laminar flow with closed streamlines at large Reynolds number. *J. Fluid Mech.* **1**, 177–190.

Benjamin, T. B. 1962 The solitary wave on a stream with an arbitrary distribution of vorticity. *J. Fluid Mech.* **12**, 97–116.

Benney, D. J. 1966 Long non-linear waves in fluid flows. *J. Math. Phys.* **45**, 52–63.

Brown, D. J. & Christie, D. R. 1998 Fully nonlinear solitary waves in continuously stratified incompressible Boussinesq fluids. *Phys. Fluids* **10**, 2569–2586.

Boussinesq, J. 1871 Théorie de l'intumescence liquid appelée onde solitaire ou de translation, se propageant dans un canal rectangulaire. *C. R. Acad. Sci. Paris* **72**, 755–759.

Byatt-Smith, J. G. & Longuet-Higgins, M. S. 1976 On the speed and profile of steep solitary waves. *Proc. R. Soc. Lond.* A **350**, 175–189.

Chavanis, P. H. & Sommeria, J. 1998 Classification of robust isolated vortices in two-dimensional hydrodynamics. *J. Fluid Mech.* **356**, 259–296.

Craik, A. D. D. 1985 *Wave Interactions and Fluid Flows.* Cambridge University Press.

Delachenal, M. B. 1973 Existence d'écoulement permanent de type coin pour un fluide parfait a surface libre. *C. R. Acad. Sci. Paris* **276**, 1021–1024.

Derzho, O. G. & Grimshaw, R. H. J 1997 Solitary waves with a vortex core in a shallow layer of stratified fluid. *Phys. Fluids* **9**, 3378–3385.

Fenton, J. D. 1972 A ninth-order solution for the solitary wave. *J. Fluid Mech.* **53**, 257–271.

Flierl, G. R. 1987 Isolated eddy models in geophysics. *Annu. Rev. Fluid Mech.* **19**, 493–530.

Freeman, N. G. & Johnson, R. S. 1970 Shallow water waves on shear flows. *J. Fluid Mech.* **42**, 401–409.

Grimshaw, R. 1971 The solitary wave in water of variable depth. Part 2. *J. Fluid Mech.* **46**, 611–622.

Izrar, B. & Lusseyran, F. & Miroshnikov, V. 1995 Two-level solitary waves as generalized solutions of the KdV equation. *Phys. Fluids* **7**, 1056–1062.

Hunter, J. K. & Vanden-Broeck, J.-M. 1983 Accurate computations for steep solitary waves. *J. Fluid Mech.* **136**, 63–71.

Johnson, R. S. 1997 *A Modern Introduction to the Mathematical Theory of Water Waves.* Cambridge University Press.

Karabut, E. A. 1996 Asymptotic expansions in the problem of a solitary wave. *J. Fluid Mech.* **319**, 109–123.

Keller, J. B. 1948 The solitary wave and periodic waves in shallow water. *Commun. Pure Appl. Maths* **1**, 323–339.

Kolesnikov, Yu. B. & Miroshnikov, V. A. 1992 Magnetohydrodynamic method of generating solitary waves. *Magnetohydrodyn.* **28**, 57–64.

Korteweg, D. J. & de Vries, G. 1895 On the change of form of long waves advancing in a rectangular canal and on a new type of long stationary waves. *Phil. Mag.* **39**, 422–443.

Laitone, E. V. 1960 The second approximation to cnoidal and solitary waves. *J. Fluid Mech.* **9**, 430–444.

Lamb, H. 1932 *Hydrodynamics.* Cambridge University Press.

Longuet-Higgins, M. S. 1974 On the mass, momentum, energy and circulation of a solitary wave. *Proc. R. Soc. Lond.* A **337**, 1–13.

Longuet-Higgins, M. S. & Fenton 1974 On the mass, momentum, energy and circulation of a solitary wave II. *Proc. R. Soc. Lond.* A **340**, 471–493.

Longuet-Higgins, M. S. & Fox, M. J. H. 1996 Asymptotic theory for the almost-highest solitary wave. *Proc. R. Soc. Lond.* A **317**, 1–19.

Meleshko, V. V. & van Heijst, G. J. F. 1994 On Chaplygin's investigations of two-dimensional vortex structures in an inviscid fluid. *J. Fluid Mech.* **272**, 157–182.

Milne-Thompson, L. M. 1968 *Theoretical Hydrodynamics.* Dover.

Miroshnikov, V. A. 1995 Solitary wave on the surface of a shear stream in crossed electric and magnetic fields: the formation of a single vortex. *Magnetohydrodyn.* **31**, 149–165.

Miroshnikov, V. A. 1996 The finite-amplitude solitary wave on a stream with linear vorticity. *Eur. J. Mech.* B/*Fluids* **15**, 395–411.

Miroshnikovs, V. A. 1996 Coupled solitary waves in viscous MHD and geophysical flows. *C. R. Acad. Sci. Paris* IIb **323**, 23–30.

Miroshnikov, V. 1998 Coupled viscous solitary waves in quasi-two-dimensional magnetohydrodynamical and geophysical flows. In *Progress in Fluid Flow Research: Turbulence and Applied MHD* (ed. H. Branover & Y. Unger), pp. 281–297. AIAA.

Miroshnikov, V. 1999 Flow separation in finite-amplitude solitary waves on shallow water with constant vorticity. *Bul. APS* **44**, No. 8, 90.

Pennel, S. A. 1987 On a series expansion for the solitary wave. *J. Fluid Mech.* **179**, 557–561.

Pennel, S. A. & Su, C. H. 1984 A seventeenth-order series expansion for the solitary wave. *J. Fluid Mech.* **149**, 431–443.

Peregrine, D. H. 1976 Interaction of water waves and currents. *Adv. Appl. Mech.* **16**, 9–117.

Pullin, D. I & Grimshaw, R. H. J. 1988 Finite-amplitude solitary waves at the interface between two homogeneous fluids. *Phys. Fluids* **31**, 3550–3559.

Rayleigh, lord 1876 On waves. *Phil. Mag.* **1**, 257–279.

Simmen, J. A. & Saffman, P. G. 1985 Steady deep-water waves on a linear shear current. *Stud. Appl. Maths* **73**, 35–57.

Sha, H. & Vanden-Broeck, J.-M. 1995 Solitary waves on water of finite depth with a surface or bottom shear layer. *Phys. Fluids* **7**, 1048–1055.

Teles da Silva, A. F. & Peregrine, D. H. 1988 Steep, steady surface waves on water of finite depth with constant vorticity. *J. Fluid Mech.* **195**, 281–302.

Vanden-Broeck, J.-M. 1994 Steep solitary waves in water of finite depth with constant vorticity. *J. Fluid Mech.* **274**, 339–348.

Vanden-Broeck, J.-M. 1995 New families of steep solitary waves in water of finite depth with constant vorticity. *Eur. J. Mech.* B/*Fluids* **14**, 761–774.

Vanden-Broeck, J.-M. 1996 Periodic waves with constant vorticity in water of finite depth. *IMA J. Appl. Maths* **56**, 207–217.

Williams, J. M. 1981 Periodic waves with constant vorticity in water of finite depth. *Proc. R. Soc. Lond.* A **302**, 139–188.

Witting, J. 1975 On the highest and other solitary waves. *SIAM J. Appl. Maths* **28**, 700–719.